

Topical Review

On the *in vivo* photochemical rate parameters for PDT reactive oxygen species modeling

Michele M Kim^{1,2}, Ashwini A Ghogare^{3,4}, Alexander Greer^{3,4}
and Timothy C Zhu^{1,5}

¹ Department of Radiation Oncology, University of Pennsylvania, Philadelphia, PA, United States of America

² Department of Physics and Astronomy, University of Pennsylvania, Philadelphia, PA, United States of America

³ Department of Chemistry, City University of New York, Brooklyn College, Brooklyn, NY 11210, United States of America

⁴ PhD Program in Chemistry, The Graduate Center of the City University of New York, 365 Fifth Avenue, New York, NY 10016, United States of America

E-mail: tzhu@mail.med.upenn.edu

Received 4 January 2016, revised 12 August 2016

Accepted for publication 5 September 2016

Published 6 February 2017



CrossMark

Abstract

Photosensitizer photochemical parameters are crucial data in accurate dosimetry for photodynamic therapy (PDT) based on photochemical modeling. Progress has been made in the last few decades in determining the photochemical properties of commonly used photosensitizers (PS), but mostly in solution or *in vitro*. Recent developments allow for the estimation of some of these photochemical parameters *in vivo*. This review will cover the currently available *in vivo* photochemical properties of photosensitizers as well as the techniques for measuring those parameters. Furthermore, photochemical parameters that are independent of environmental factors or are universal for different photosensitizers will be examined. Most photosensitizers discussed in this review are of the type II (singlet oxygen) photooxidation category, although type I photosensitizers that involve other reactive oxygen species (ROS) will be discussed as well. The compilation of these parameters will be essential for ROS modeling of PDT.

Keywords: PDT, reactive oxygen species, decay rates

(Some figures may appear in colour only in the online journal)

⁵ Author to whom any correspondence should be addressed.

List of symbols

α	$^3\text{O}_2$ solubility coefficient, see equation (B.3) ($\mu\text{M mmHg}^{-1}$)
α_c	$^3\text{O}_2$ solubility in plasma, see equation (B.1) ($\mu\text{M mmHg}^{-1}$)
α_t	$^3\text{O}_2$ solubility in tissue, see equation (B.4) ($\mu\text{M mmHg}^{-1}$)
β	$(k_4 + k_8[A])/k_2$, see table 2, (μM)
Γ	Rate of the oxygen loading/unloading, see equation (14) ($\mu\text{M s}^{-1}$)
δ	Low concentration correction, see table 2, equation (19) (μM)
ε	Extinction coefficient, see table 2 ($\text{cm}^{-1} \mu\text{M}^{-1}$)
η	Hypoxic reaction consumption rate, see table 2 ($\text{cm}^2 \text{mW}^{-1} \text{s}^{-1} \mu\text{M}$)
ξ	Specific oxygen consumption rate, see table 2, ($\text{cm}^2 \text{mW}^{-1} \text{s}^{-1}$)
σ	Specific photobleaching ratio, see table 2, (μM^{-1})
τ_f	Fluorescence lifetime, see table 2, (s)
τ_t	Triplet lifetime, see table 2, (s)
τ_Δ	Singlet oxygen lifetime, see table 2, (s)
ϕ	Fluence rate, see equation (20), (mW cm^{-2})
Φ_f	Fluorescence quantum yield, see table 2
Φ_t	Triplet quantum yield, see table 2
Φ_Δ	Singlet oxygen quantum yield, see table 2
Φ_{ROS}	Superoxide anion quantum yield, see table 2
[A]	Biological substrates that are singlet oxygen receptors, see table 2, equation (9) (μM)
C_H	Hemoglobin concentration in blood, see equation (B.2) (μM)
D_c	$^3\text{O}_2$ diffusion coefficient in capillary, see equation (B.1) ($\mu\text{m}^2 \text{s}^{-1}$)
D_H	Hemoglobin diffusion coefficient, see equation (B.2) ($\mu\text{m}^2 \text{s}^{-1}$)
D_s	$^3\text{O}_2$ diffusion coefficient in vascular media, see equation (B.5) ($\mu\text{m}^2 \text{s}^{-1}$)
D_t	$^3\text{O}_2$ diffusion coefficient in tissue, see equation (B.4) ($\mu\text{m}^2 \text{s}^{-1}$)
g	Oxygen perfusion rate, see table 2, equation (18) ($\mu\text{M s}^{-1}$)
k_0, k_a	Photon absorption rate of photosensitizer per photosensitizer concentration, $k_0 = \varepsilon\phi/h\nu$, see table 1, equations (1) and (29) (s^{-1})
k_1, k_{os}	Bimolecular rate for $^1\text{O}_2$ (k_{12}) and ROS (k_{11}) reactions with ground-state photosensitizer, see table 1, equation (2) ($\mu\text{M}^{-1} \text{s}^{-1}$)
k_2, k_{ot}	Bimolecular rate of triplet photosensitizer quenching by $^3\text{O}_2$, see table 1, equation (3) ($\mu\text{M}^{-1} \text{s}^{-1}$)
k_3, k_f	Decay rate of first excited singlet state photosensitizer to ground state photosensitizer, $k_3 = k_{3\text{NR}} + k_{3\text{R}}$, see table 1, equation (1) (s^{-1})
$k_{3\text{NR}}$	Non-radiative (spontaneous) decay rate of first excited singlet state photosensitizer to ground state photosensitizer, see table 2, equation (1) (s^{-1})
$k_{3\text{R}}$	Radiative (fluorescence) rate of monomolecular decay of the first excited singlet state photosensitizer to ground state photosensitizer, see equation (1) (s^{-1})
k_4, k_p	Phosphorescence decay rate of the photosensitizer triplet state to ground state, $k_4 = k_{4\text{NR}} + k_{4\text{R}}$, see table 1, equation (6) (s^{-1})
$k_{4\text{NR}}$	Non-radiative rate of monomolecular decay of the photosensitizer triplet state, see equation (42) (s^{-1})
$k_{4\text{R}}$	Radiative rate of monomolecular decay of the photosensitizer triplet state, see equation (42) (s^{-1})
k_5, k_{isc}	Intersystem crossing rate of first excited photosensitizer to triplet state photosensitizer, see table 1, equation (7) (s^{-1})
k_6, k_d	$^1\text{O}_2$ to $^3\text{O}_2$ phosphorescence decay rate, see table 1, equation (8) (s^{-1})

k_7, k_{oa}	Bimolecular rate of reaction of 1O_2 with biological substrate [A], see table 1, equation (9) ($\mu M^{-1} s^{-1}$)
k_8, k_{ta}	Bimolecular rate of reaction of T_1 with biological substrate [A], see table 1, equation (10) ($\mu M^{-1} s^{-1}$)
k_q	Physical quenching rate of 1O_2 by substrate [A], see equation (41), (s^{-1})
k_r	Chemical quenching rate of 1O_2 by substrate [A], see equation (41), (s^{-1})
P	Oxygen partial pressure, see equation (B.3) (mmHg)
P_m	Oxygen partial pressure at half maximum oxygen consumption concentration, see equation (B.4) (mmHg)
q_0	3O_2 maximum metabolic consumption rate, see equation (B.4), ($\mu M s^{-1}$)
S_0	Photosensitizer in its ground state, see figure 2
S_1	Photosensitizer in its first singlet state, see figure 2
S_Δ	Fraction of triplet-state photosensitizer- 3O_2 reactions to produce 1O_2 , see table 2
S_I	Fraction of triplet state photosensitizer- 3O_2 reactions that involve type I reactions, see table 2
S_{NL}	Fraction of triplet state photosensitizer reactions that are non-luminescent, see table 2
Sa (SaO ₂)	Hemoglobin oxygen saturation, see equation (B.2)
T_1	Photosensitizer in its first triplet state, see figure 2
v	Velocity of blood flow, see equations (B.1) and (B.2) ($\mu m s^{-1}$)

1. Introduction

Photodynamic therapy (PDT) is a treatment modality for malignant and non-malignant diseases that uses visible light to activate photosensitizers (PS) to generate cytotoxic oxygen species to kill cancer cells (Dougherty 1993). PDT has been approved by the US Food and Drug Administration for the treatment of microinvasive lung cancer, obstructing lung cancer, and obstructing esophageal cancer, as well as for premalignant actinic keratosis and age-related macular degeneration (Huang 2005, Wilson and Patterson 2008, Zhu and Finlay 2008, Agostinis *et al* 2011, Simone *et al* 2012, Pogue *et al* 2016).

PDT is not only 'dynamic' but also multifaceted. There are three principal components: photosensitizer, light, and oxygen, all of which interact on time scales relevant to a single treatment. The distribution of light is determined by the light source characteristics and the tissue optical properties. The tissue optical properties, in turn, are influenced by the concentration of photosensitizer and the concentration and oxygenation of the blood. The distribution of oxygen is altered by the photodynamic process, because it consumes oxygen, thus affecting the ingress of oxygen diffusion into tissue. The distribution of photosensitizer can be modeled as a diffusion process through the vasculature for most PS. Some, such as 5-aminolevulinic acid (ALA), induce the production of protoporphyrin IX (PpIX), which is governed by the concentration of free heme (Kennedy and Pottier 1992). Finally, distribution of the photosensitizer may change as a result of photobleaching, which is the photodynamic destruction of the photosensitizer itself. To account for these interactions, a dynamic model of the photodynamic process is required.

Two types of photosensitized oxidation, named type I and type II, have emerged, as shown in figure 1 (Foote 1976, 1991, Adam 1981, Ranby 1981, Greer 2006, Cadet *et al* 2008). Both reactions involve the absorption of light by a photosensitizer ($[S_0]$) to produce an excited-state photosensitizer ($[S_1]$) (Foote 1991).

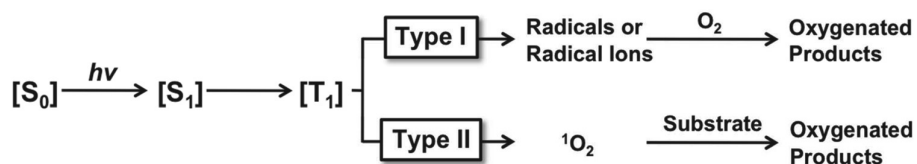


Figure 1. Type I and type II photosensitized oxidations. The type I pathway produce radicals or radical ions, which in subsequent reactions produce ROS. The type II pathway is primarily due to energy transfer from an excited photosensitizer to triplet oxygen to produce singlet oxygen.

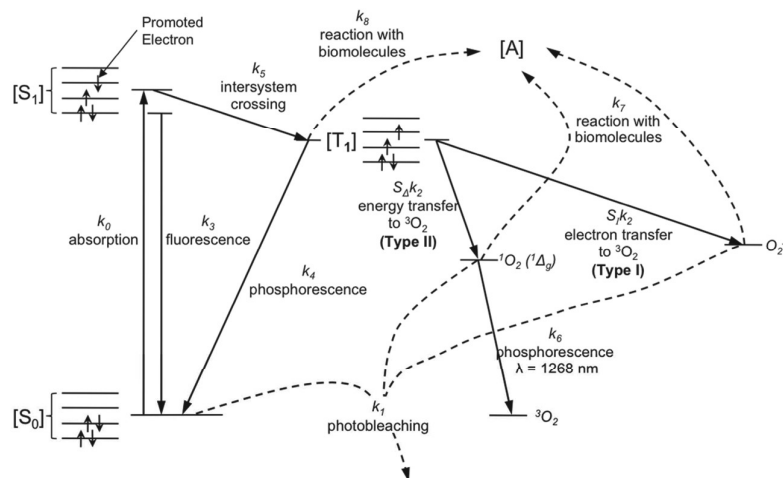


Figure 2. Diagram for the photoactivation of photosensitizer in the presence of oxygen and biomolecules. The photosensitizer in its ground state (S_0) absorbs a photon and is excited to its first singlet state (S_1). It converts to its excited triplet state (T_1) via intersystem crossing (ISC). From T_1 , energy is transferred to ground state molecular oxygen (3O_2), creating reactive singlet oxygen (1O_2) for a typical type II reaction. In type I reactions, the triplet photosensitizer will transfer an electron to 3O_2 which will react with molecular targets to produce radical species, or alternatively interact directly with the acceptor, [A], without oxygen mediation. k_3 and k_4 include both radiative and non-radiative decay rates for fluorescence and phosphorescence, respectively (see table 1).

The type I mechanism involves hydrogen atom or electron transfer, yielding radicals or radical ions (Foote 1991, Greer 2006, Ghogare and Greer 2016). The triplet state photosensitizer can also react directly with an organic molecule or substrate, but this is not classified as a photosensitized oxidation. Here, the substrate can donate an electron to the photosensitizer, creating a substrate radical cation and a photosensitizer radical anion (Simone *et al* 2012). This process can occur in hypoxic conditions, but in the presence of oxygen, the triplet photosensitizer can undergo an electron transfer with molecular oxygen to generate superoxide anions (O_2^-) (Sharman *et al* 2000). The radicals formed can react with each other to chain terminate or with other molecules (such as the molecular target or the solvent) to form other radical species leading to secondary reactions leading to oxygenated compounds (Gollnick 1968, Sharman *et al* 2000, Simone *et al* 2012). Superoxide anion is not very reactive in biological systems, but it can react with water to form hydrogen peroxide (H_2O_2). H_2O_2 easily

passes through biological membranes, and since it is not restricted to one cellular component, it is quite relevant in causing cellular damage. Figure 2 shows the two pathways of a type I interaction—one via triplet state photosensitizer interacting with [A] directly without any oxygen mediation and one via an electron transfer to oxygen to form the superoxide anion (O_2^-).

Most PS used in the clinic are of the type II category, which produce singlet oxygen as the main photocytotoxic agent for events that eventually cause cell death and/or therapeutic effects (Foote 1976, Weishaupt *et al* 1976, Zhu and Finlay 2008, Douki *et al* 2002). In contrast to type I reactions, such as electron transfer to oxygen, in type II reactions, the photosensitizer triplet state, [T_1], transfers energy to molecular oxygen to generate 1O_2 . During PDT, as shown in figure 2, photosensitizer is excited by light at a certain wavelength matching the absorption energy gap to the excited state [S_1] from its ground state [S_0]. Both this state and the ground state are spectroscopic singlet states. One essential property of a good photosensitizer is a high intersystem crossing (ISC) yield, i.e. a high probability of transition from (S_1) to a triplet state (T_1). In the T_1 state, the photosensitizer can transfer energy to molecular oxygen (3O_2), exciting it to its highly reactive singlet state (1O_2). Ideal photosensitizer properties and experimental conditions that favor the singlet oxygen (type II) pathway include (i) a high extinction coefficient (ϵ), (ii) a high triplet quantum yield of the photosensitizer ($\Phi_t \sim 1$), and (iii) a low chemical reactivity of the photosensitizer triplet state ($k_8 \sim 0$). Competition between type I and II photooxidation chemistry is inevitable upon the formation of an excited photosensitizer in the presence of 3O_2 . For Rose Bengal, singlet oxygen (1O_2) is a key reactive species produced in PDT, where estimates place the singlet oxygen contribution at ~80%, and hydroxyl radical and other reactive oxygen species (ROS) at ~20% (Pouget *et al* 2000). Photosensitizer properties and the concentration of oxygen present in the environment will be an important factor in determining the ratio between the two types of reactions (Plaetzer *et al* 2009).

2. Impact of dosimetry to clinical PDT

Explicit PDT dosimetry has been performed in pre-clinical and clinical applications. Among the three components (light, photosensitizer (PS), and oxygen), much work has focused on the measurement of the light fluence and PS concentration. Oxygen transport and consumption during PDT remain important for the modeling of ROS generation. Currently available methods to measure tissue oxygenation concentration are still in the pre-clinical stage. The macroscopic model described in section 3 can be used to calculate the ROS concentration (see equation (27)) based on explicit dosimetry measurements of light fluence and PS concentration. Current state of the art of clinical PDT prescriptions use the product of the drug concentration and light fluence, also called PDT dose.

Pre-clinical mouse studies were performed to compare the correlation of the dosimetric metrics (total light fluence, PDT dose, calculation of reacted singlet oxygen) and PDT efficacy (Penjweini *et al* 2015a, Kim *et al* 2015, Qiu *et al* 2016). Figure 3 shows the comparison between the PDT dose metrics and PDT outcome for BPD-mediated PDT in RIF tumor bearing mice. Cure index, $CI = [1 - (\text{tumor growth rate})/(\text{control tumor growth rate})]$, was used as a measure of tumor control by PDT: $CI = 0$ no PDT effect; $CI = 1$ complete PDT cure. It is clear that the correlation is progressively improving from total fluence (figure 3(a)), PDT dose (figure 3(b)), to reacted singlet oxygen, $[^1O_2]_{rx}$ (figure 3(c)), as the grey uncertainty of the correlation reduces with the corresponding goodness of fit $R^2 = 0.73, 0.93, \text{ and } 0.99$, respectively.

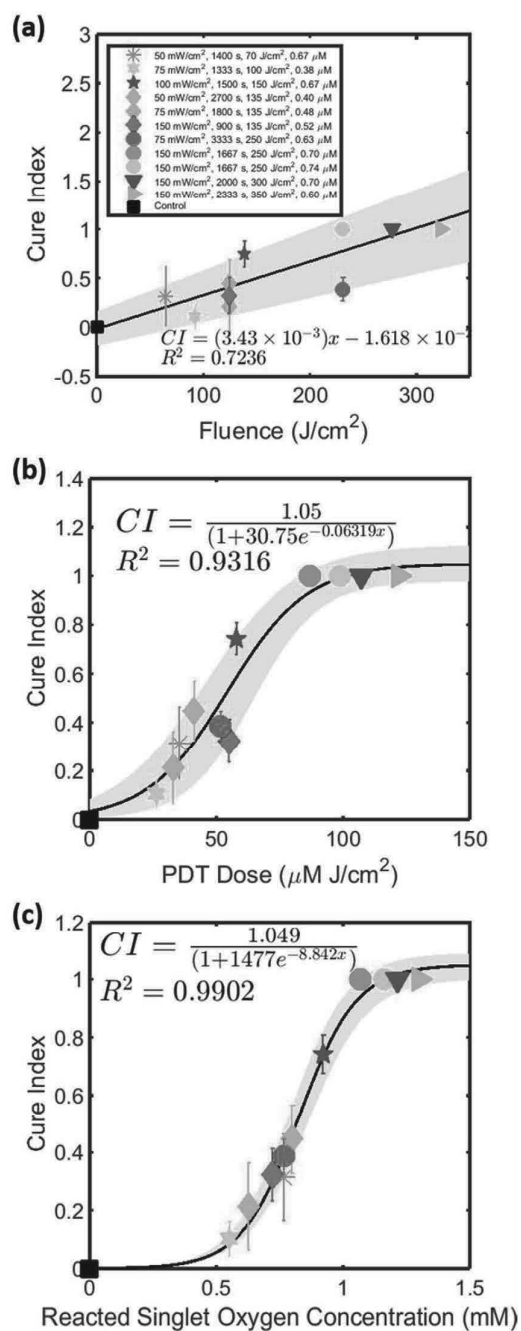


Figure 3. Cure index versus (a) light fluence (b) PDT dose and (c) calculated reacted singlet oxygen for BPD mediated PDT in RIF tumor. The grey regions indicate the 95% confidence intervals of the fitted line (in black). The goodness of the fit, R^2 , is also shown.

3. Type I and II photosensitized oxidation reactions

3.1. Photochemical reactions

The PDT kinetics process was described using rate equations in the literature for microscopic and macroscopic models (Wilkinson and Brummer 1981, Foster *et al* 1991, Hu *et al* 2005, Zhu *et al* 2007). The PDT process is started by the absorption of light by the photosensitizer in the ground state, S_0 . It is excited into the singlet state, S_1 . The S_1 state can spontaneously decay to the ground state with the emission of a photon or heat (Zhu *et al* 2007)



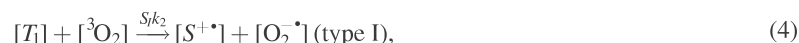
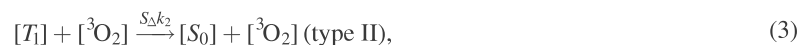
This is a reversible process. The monomolecular absorption rate, k_0 (s^{-1}), is proportional to the light fluence, ϕ , and the extinction coefficient, ε . The monomolecular decay rate, k_3 (s^{-1}) is the rate from S_1 to S_0 . The decay rate due to fluorescence (radiative) is k_{3R} (s^{-1}) and the internal conversion (non-radiative) decay rate is k_{3NR} (s^{-1}), so that $k_3 = k_{3NR} + k_{3R}$ (Sternborg and van Gemert 1996). The photosensitizer in its ground state can interact with singlet oxygen and ROS to form a photoproduct $[SO_2]$. This can be described by the decay rate constant, $k_1 = k_{11} + k_{12}$ ($\mu M^{-1} s^{-1}$)



and



Similarly, the bimolecular decay rate, k_2 ($\mu M^{-1} s^{-1}$), describes the rate of interactions by collisions between the triplet state photosensitizer $[T_1]$ and ground state oxygen $[^3O_2]$. A fraction (S_Δ) of the interactions yields singlet oxygen (equation (3)), while another fraction (S_I) yields the superoxide anion ($O_2^{\cdot-}$) as in (4)



The last equation shows the fraction ($S_{NL} = 1 - S_\Delta - S_I$) of the interactions between the triplet state photosensitizer and ground state oxygen to produce non-luminescent decay of $[T_1]$ and do not yield singlet oxygen and/or superoxide anion. Physical quenching can also occur where singlet oxygen is converted back to triplet oxygen ($^1O_2 \rightarrow ^3O_2$) (Foote 1991). S_I is the fraction of interactions of $[T_1]$ that produce type I reactions.

Triplet decay rate and ISC of the photosensitizer are described by the monomolecular reaction rates k_4 and k_5 (s^{-1}), respectively. The triplet decay rate includes both the radiative (k_{4R}) and non-radiative (k_{4NR}) decay rate constants

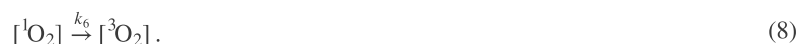


Table 1. Definition of photochemical reaction rate constants.

Symbol ^a	Definition
k_0, k_a (s^{-1})	Photon absorption rate of photosensitizer as a function of photosensitizer concentration (in μM), $k_0 = \epsilon\phi/h\nu$, for $\phi = 100 \text{ mW cm}^{-2}$.
k_1, k_{os} ($\mu M^{-1} s^{-1}$)	Bimolecular decay rate for 1O_2 (k_{12}) and ROS (k_{11}) reactions with ground-state photosensitizer
k_2, k_{ot} ($\mu M^{-1} s^{-1}$)	Bimolecular decay rate of triplet photosensitizer quenching by 3O_2 $S_I k_2$ Reactions involving triplet state and electron transfer to 3O_2 (type I) $S_{\Delta} k_2$ Reactions involving triplet state and energy transfer to 3O_2 (type II) $S_{NL} k_2$ Reactions involving triplet state that are non-luminescent
k_3, k_f (s^{-1})	Fluorescence decay rate of first excited singlet state photosensitizer to ground state photosensitizer including internal conversion (non-radiative, k_{3NR}) and fluorescent (radiative, k_{3R}) terms
k_4, k_p (s^{-1})	Phosphorescence decay of the photosensitizer triplet state to ground state photosensitizer, including radiative (k_{4R}) and non-radiative (k_{4NR}) components
k_5, k_{isc} (s^{-1})	Intersystem crossing (ISC) rate from first excited photosensitizer to triplet state photosensitizer
k_6, k_d (s^{-1})	Phosphorescence (or luminescence) decay rate of 1O_2 to 3O_2
k_7, k_{oa} ($\mu M^{-1} s^{-1}$)	Bimolecular decay rate of reaction of type II 1O_2 (k_{72}) and type I ROS (k_{71}) with biological substrate [A]
k_8, k_{1a} ($\mu M^{-1} s^{-1}$)	Bimolecular decay rate constant for reaction of triplet photosensitizer with substrate [A] for type I reactions

^a The first symbol is used in this paper. The second symbol is also commonly found in the literature.

The phosphorescence (or luminescence) of singlet oxygen is described by the monomolecular decay rate k_6 (s^{-1})



This reaction produces the signature luminescence at 1270 nm. However, there are also non-luminescent reactions of 1O_2 , such as solvent quenching or physical quenching of 1O_2 , mentioned above and described next in section 3.1.1 (Wilkinson *et al* 1993).

The oxidation of biomolecular acceptors, [A], is described by the decay rate $k_7 = k_{71} + k_{72}$ (s^{-1})



and



Table 1 summarizes the definition of all rate constants used here along with their conventional names.

3.1.1. Kinetics of type I reactions. Type I photooxidation reactions are described by the bimolecular reaction rate $S_I k_2$ ($\mu M^{-1} s^{-1}$) with the fraction of triplet interactions that lead to type I reactions (equation (4)). In a type I reaction, the photosensitizer can undergo electron transfer with oxygen to generate a superoxide anion ($O_2^{\bullet-}$). Superoxide anion, its protonated form HO_2^{\bullet} and other radicals such as hydroxyl radicals (HO^{\bullet}) readily cause cell damage (see figure 4). Notice that even though ROSs can be generated by the superoxide anion ($O_2^{\bullet-}$) from a type I photosensitizer, there are many additional pathways to generate ROS that are not all included in figure 4. Details of which can be found elsewhere (Plaetzer *et al* 2009).

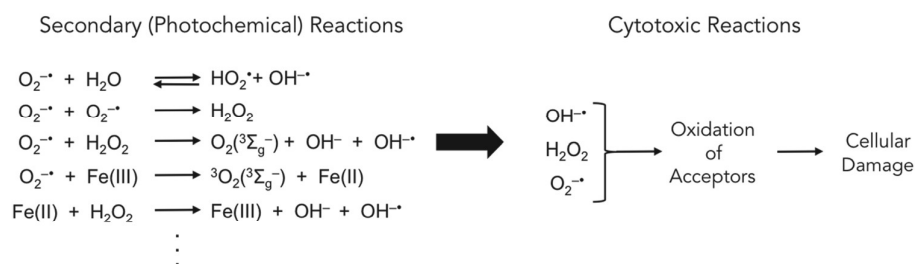


Figure 4. Secondary (photochemical) reactions for type I photosensitizer to generate the resulting reactive oxygen species ($\text{OH}^{\cdot-}$, H_2O_2 , $\text{O}_2^{\cdot-}$). Other redox active metals may be pertinent for generation of ROS and should be included as part of secondary reactions in ‘...’. ROS will in turn oxidate acceptors in cells to cause cellular damage. $\text{OH}^{\cdot-}$ and HO^{\cdot} have been used interchangeably in the text.

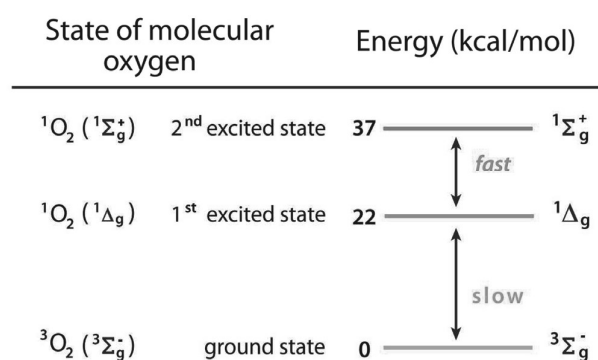


Figure 5. Energy diagram of triplet ground-state $\text{O}_2 (^3\Sigma_g^-)$, excited singlet delta ($^1\Delta_g$) and excited singlet sigma ($^1\Sigma_g^+$) state of oxygen.

For simplicity, we have lumped these interactions as direct interaction with superoxide anion (equation (9b)). Other reactions involve the reaction of the triplet state [T_1] with the molecular substrate directly, described by the reaction rate k_8 ($\mu\text{M}^{-1} \text{s}^{-1}$)



3.1.2. Kinetics of type II reactions.

Diatomic oxygen energy states. The electronic behavior of molecular oxygen results from the arrangement of two electrons in the outer π_g shell (it has a total of 16 electrons since $Z = 8$ for each O atom) (Kasha 1985, Greer *et al* 2014). Molecular oxygen has an electron configuration in which orbitals are designated as even parity ($g = \text{gerade}$) or odd parity ($u = \text{ungerade}$)

$$(1\sigma_g)^2(2\sigma_u)^2(2\sigma_g)^2(2\sigma_u)^2(3\sigma_g)^2(1\pi_u)^4(1\pi_g)^2$$

where the π_g orbital (formally an open shell) has three possible electron spin arrangements giving rise to three energetically different species: $^3\Sigma_g^-$, $^1\Delta_g$ and $^1\Sigma_g^+$ (figure 5). Ground state molecular oxygen ($^3\Sigma_g^-$) is a triplet ($l = 1$) and biradical in character; while the two singlet

states ($l = 0$) ${}^1\Delta_g$ and ${}^1\Sigma_g^+$ both exist on excited surface. The first excited state (${}^1\Delta_g$) is located 22 kcal mol^{-1} (0.954 eV , $\lambda = 1270 \text{ nm}$) above the ground state with electrons paired in oxygen's degenerate π antibonding orbitals. A valence bond treatment can also be considered: The ionic resonance structures for dioxygen, O^+-O^- and equally contributing O^--O^+ for ${}^1\Delta_g$, are unimportant compared to ground-state triplet for O_2 because of the positive charge on oxygen. The second singlet excited state (${}^1\Sigma_g^+$) is located 37 kcal mol^{-1} (1.6 eV , $\lambda = 755 \text{ nm}$) above the ground state. Quenching of the excited PS of a high enough energy by the ground state molecular oxygen produces both forms of singlet oxygen (Greer *et al* 2014). Because ${}^1\Delta_g$ oxygen lifetimes are in the microsecond range they can undergo bimolecular reactions; in contrast, the ${}^1\Sigma_g^+$ oxygen lifetime is short (due to the faster interconversion to ${}^1\Delta_g$ oxygen) (Weldon *et al* 1999) and thus chemically unreactive.

Photosensitization routes to ${}^1\Delta_g$ and ${}^1\Sigma_g^+$ are of interest. However, the longer lifetime of ${}^1\Delta_g$ oxygen relates to its chemical reactivity. Chemical reactivity has been generated for ${}^1\Delta_g$ oxygen with biomolecules. Consequently, bimolecular reaction rates for the disappearance of and oxidation by ${}^1\Delta_g$ oxygen (labeled as ${}^1\text{O}_2$ in this paper) are available.

The reactions of singlet oxygen with substrates can be defined by the rate constants (k_7 , k_6). k_{72} (also commonly called k_{oa}) is the total reaction rate constant which gives the total rate of disappearance of ${}^1\text{O}_2$ induced by substrate both chemically and physically ($k_{\text{oa}} = k_q + \gamma k_r$), where k_q is the physical quenching (quenching of ${}^1\text{O}_2$ due to an interaction with another molecule) rate constant, and k_r is the chemical reaction rate constant of ${}^1\text{O}_2$ which accounts for the rate of formation of oxygenated products. The variable γ relates to the consumption of the product. k_6 (also commonly called k_d) is rate constant for natural decay of ${}^1\text{O}_2$ back to ${}^3\text{O}_2$ (also called solvent quenching). For example, amines efficiently deactivate ${}^1\text{O}_2$ back to ${}^3\text{O}_2$ by charge-transfer quenching and carotenoids efficiently deactivate ${}^1\text{O}_2$ back to ${}^3\text{O}_2$ by energy-transfer quenching (Rodgers and Lee 1984, Catalan *et al* 2003, Musbat *et al* 2013, Lambert and Redmond 1994).

In vivo photochemical reactions of singlet oxygen. Over the past five decades, the reactivity of ${}^1\text{O}_2$ has been explored. Singlet oxygen reacts with compounds and biological material to give oxygenated products, such as endoperoxides from [2 + 4] cycloadditions, dioxetanes from [2 + 2] cycloadditions, oxides from heteroatom oxidations, hydroperoxides from 'ene' reactions and tandem ${}^1\text{O}_2$ reactions (Turro *et al* 2010, Zamadar and Greer 2010, Stratakis and Orfanopoulos 2000, Vassilikogiannakis *et al* 2005, Kotzabasaki *et al* 2016). Reactions of singlet oxygen with small biomolecules have been carried out. For example, mechanisms have been studied such as the photooxidation of bilirubin and guanosine and ascorbic acid derivatives. Examples of ${}^1\text{O}_2$ reactions in the organic chemistry that are models of biological reactions are listed in Appendix A, where the rate constants of small molecule reactions provide some insight to an overall photooxidative outcome in a biological system.

Chemical trapping of ${}^1\text{O}_2$ is known in solution with biomolecules. The reactivity of ${}^1\text{O}_2$ with biomolecules (e.g. membranes and lipids), amino acids (e.g. His, Trp, and Met), and nucleic acids (e.g. guanosine) as model systems help in understanding the mechanism of toxicity in PDT (Kanofsky 1989, Girotti 2001, McDonagh 2001, Cadet *et al* 2006, Itri *et al* 2014). Reaction of ${}^1\text{O}_2$ with methionine is an example of heteroatom oxidation in proteins (figure 6). For methionine, two moles of methionine sulfoxide form per mole of ${}^1\text{O}_2$ in the reaction ($\gamma = 2$). Certain biomolecules such as amines and carotenes can serve as protection against singlet oxygenation in converting ${}^1\text{O}_2$ to ${}^3\text{O}_2$ by physical quenching (as was mentioned above).

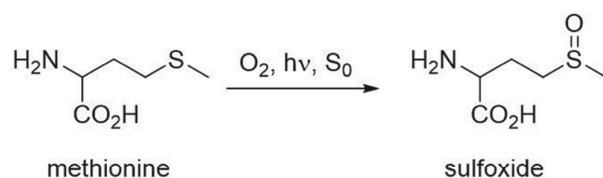


Figure 6. Reaction of methionine with $^1\text{O}_2$ to form sulfoxide.

3.2. Explicit model of type I and II photodynamic interactions

For both type I and II primary photochemical reactions, as explained in section 3.1, a set of coupled differential equations can be used to describe the PDT process (Finlay *et al* 2001, Wang *et al* 2007, 2010, Zhu *et al* 2007, Weston and Patterson 2011)

$$\frac{d[S_0]}{dt} = -k_0[S_0] - k_{12}[^1\text{O}_2]([S_0] + \delta) - k_{11}[\text{O}_2^-]([S_0] + \delta) + k_2[T_1][^3\text{O}_2] + k_3[S_1] + k_4[T_1], \quad (11)$$

$$\frac{d[S_1]}{dt} = -(k_3 + k_5)[S_1] + k_0[S_0], \quad (12)$$

$$\frac{d[T_1]}{dt} = -k_2[T_1][^3\text{O}_2] - k_4[T_1] + k_5[S_1] - k_8[T_1][A], \quad (13)$$

$$\frac{d[^3\text{O}_2]}{dt} = -S_\Delta k_2[T_1][^3\text{O}_2] - S_I k_2[T_1][^3\text{O}_2] + k_6[^1\text{O}_2] + \Gamma, \quad (14)$$

$$\frac{d[^1\text{O}_2]}{dt} = -k_{12}[^1\text{O}_2]([S_0] + \delta) + S_\Delta k_2[T_1][^3\text{O}_2] - k_6[^1\text{O}_2] - k_{72}[A][^1\text{O}_2], \quad (15)$$

$$\frac{d[\text{O}_2^-]}{dt} = -k_{11}[\text{O}_2^-]([S_0] + \delta) + S_I k_2[T_1][^3\text{O}_2] - k_{71}[A][\text{O}_2^-], \quad (16)$$

$$\frac{d[A]}{dt} = -k_{72}[A][^1\text{O}_2] - k_{71}[A][\text{O}_2^-] - k_8[T_1][A]. \quad (17)$$

These equations are based on the kinetic equations of the photochemical reactions using their rate constants, k_0, \dots, k_8 (see their definitions in table 1). Here, $[S_0]$, $[S_1]$, and $[T_1]$ are the ground, first excited singlet, and triplet photosensitizer concentrations respectively. $[^3\text{O}_2]$ and $[^1\text{O}_2]$ are the ground triplet and excited singlet state oxygen concentrations. $[\text{O}_2^-]$ is the concentration of superoxide anion and represents the amounts of ROS in a type I mechanism. Γ and $[A]$ are the oxygen supply rate and the concentration of ($^1\text{O}_2$ and ROS) acceptors excluding the photosensitizer molecule. Depending on the methods used to determine the oxygen supply rate in (14), the model is divided into microscopic and macroscopic models. In the microscopic model, oxygen diffusion into capillaries, from capillaries into tissue, and diffusion within tissue is used to calculate the Γ term (Wang *et al* 2007). For more details on the microscopic singlet oxygen model, see appendix B. Based on the kinetic equations of the photochemical reactions, the oxygen supply term in a macroscopic theory can be expressed as: (Hu *et al* 2005, Zhu *et al* 2007, 2015c, Wang *et al* 2010)

$$\Gamma = g \left(1 - \frac{[{}^3\text{O}_2]}{[{}^3\text{O}_2]_0} \right), \quad (18)$$

where g is the macroscopic maximum oxygen supply rate and $[{}^3\text{O}_2]_0$ is the initial tissue oxygen concentration. In the macroscopic model, the Γ term is assumed to be uniformly distributed everywhere without consideration of oxygen diffusion through the vasculature. The functional form of equation (18) was validated using forward calculations with standard vascular parameters (Zhu *et al* 2015c). Since the spatial scale of light transport is much larger than the spatial scale of oxygen diffusion (~ 1 mm versus ~ 65 μm), the light fluence rate was also set to be a constant within the vasculature model (Zhu and Liu 2013, Zhu *et al* 2015c). This term ensures that the oxygen level does not exceed the initial value.

Due to the short lifetime and diffusion distance of ${}^1\text{O}_2$ in biological media, the term for the photobleaching kinetics for ground state photosensitizer undergoing ${}^1\text{O}_2$ -mediated bleaching has the low concentration correction constant, δ (Finlay *et al* 2004, Moan and Berg 1991). ${}^1\text{O}_2$ is generated at the site of the parent photosensitizer molecule. Due to the short diffusion distance (10–100 nm (Moan and Berg 1991, Niedre *et al* 2002)), it has a higher probability of reacting with the parent photosensitizer molecule than with adjacent photosensitizer molecules. For low photosensitizer concentrations, the rate of photobleaching depends only on the rate of ${}^1\text{O}_2$ generation because the volume through which each ${}^1\text{O}_2$ can diffuse before reacting will contain exactly one photosensitizer molecule, independent of the total photosensitizer concentration. In other words, δ is the concentration of $[S_0]$ where intermolecular distance is equal to the ${}^1\text{O}_2$ diffusion distance (Dysart *et al* 2005). The value of this critical low photosensitizer concentration is estimated to be between 3 and 3000 μM (Dysart and Patterson 2005). δ can be expressed as

$$\delta = \frac{1}{d^3 N_A}. \quad (19)$$

Here, d is the diffusion distance of ${}^1\text{O}_2$ in the environment of interest, which can be related to τ_Δ by $d = (6D\tau_\Delta)^{1/2}$, where D is the diffusion coefficient for ${}^1\text{O}_2$ and N_A is Avogadro's number (Dysart *et al* 2005).

If one only cares about the dynamic process of PDT in the time scale of a few seconds to hours, then the time derivative in the right hand sides of equations (12), (13), (15) and (16) can be set to zero because these processes are known to be very fast ($\sim \mu\text{s}$ or less). They can then be simplified to

$$[S_1] = \tau_I \frac{\varepsilon}{h\nu} \phi [S_0], \quad (20)$$

$$[T_1] = \frac{\Phi_t}{[{}^3\text{O}_2] + \beta} \frac{1}{k_2} \frac{\varepsilon}{h\nu} \phi [S_0], \quad (21)$$

$$[{}^1\text{O}_2] = \xi_{II} \tau_\Delta \frac{[{}^3\text{O}_2]}{[{}^3\text{O}_2] + \beta} \phi [S_0], \quad (22)$$

$$[\text{O}_2^-] = \xi_I \tau_S \frac{[{}^3\text{O}_2]}{[{}^3\text{O}_2] + \beta} \phi [S_0], \quad (23)$$

$$\frac{d[S_0]}{dt} = -\frac{[{}^3\text{O}_2]}{[{}^3\text{O}_2] + \beta} \xi \sigma ([S_0] + \delta) \phi [S_0] - \eta \frac{1}{[{}^3\text{O}_2] + \beta} \phi [S_0], \quad (24)$$

$$\frac{d[{}^3\text{O}_2]}{dt} = -\frac{[{}^3\text{O}_2]}{[{}^3\text{O}_2] + \beta} \phi [S_0] (\xi_{\text{II}}(\sigma_{\text{II}}([S_0] + \delta) + k_{72}[A]\tau_{\Delta}) + \xi_{\text{I}}) + g \left(1 - \frac{[{}^3\text{O}_2]}{[{}^3\text{O}_2](t=0)} \right), \quad (25)$$

$$\frac{d[A]}{dt} = -\frac{[{}^3\text{O}_2]}{[{}^3\text{O}_2] + \beta} \phi [S_0] (\xi_{\text{II}} k_{72}[A]\tau_{\Delta} + \xi_{\text{I}}) - \eta \frac{1}{[{}^3\text{O}_2] + \beta} \phi [S_0]. \quad (26)$$

All of the parameters (ξ , ξ_{I} , ξ_{II} , σ , σ_{I} , σ_{II} , τ_{I} , τ_{Δ} , τ_{S}) have been defined in table 2. *In vivo*, $(\xi_{\text{II}}(\sigma_{\text{II}}([S_0] + \delta) + k_{72}[A]\tau_{\Delta}) + \xi_{\text{I}})$ in equation (25) and $(\xi_{\text{II}} k_{72}[A]\tau_{\Delta}) + \xi_{\text{I}}$ in equation (26) can be replaced with $(\xi = \xi_{\text{II}} + \xi_{\text{I}})$ since $k_{72}[A]\tau_{\Delta} \approx 1$ and $\sigma_{\text{II}}([S_0] + \delta) \ll 1$. Utilizing equation (26) above, the amount of biological acceptor that has reacted with a reactive oxygen species ($[\text{ROS}]_{\text{rx}}$) can be defined by the following

$$\frac{d[\text{ROS}]_{\text{rx}}}{dt} = -f \xi \frac{[{}^3\text{O}_2]}{[{}^3\text{O}_2] + \beta} \phi [S_0] - \eta \frac{1}{[{}^3\text{O}_2] + \beta} \phi [S_0], \quad (27)$$

where f is the fraction of ROS interacting with $[A]$. Here, the first term relates to the fraction of acceptors that reacted due to (ROS)-mediated reactions, and the second term relates to the fraction that reacts under hypoxic conditions or any other non-oxygen-mediated reactions, such as triplet interactions. In cases where type II reactions dominate ($S_{\Delta} \gg S_{\text{I}}$ and $\eta = 0$), the reacted singlet oxygen ($[{}^1\text{O}_2]_{\text{rx}}$) can be defined by

$$\frac{d[{}^1\text{O}_2]_{\text{rx}}}{dt} = -f \left(\xi \frac{\phi [S_0] [{}^3\text{O}_2]}{[{}^3\text{O}_2] + \beta} \right). \quad (28)$$

The required photochemical parameters can be reduced from 11 (δ , g , k_0 , \dots , k_8) to 6 (δ , β , ξ , σ , η , g), with some of the latter expressed as ratios of the former, if one is not interested in modeling $[S_1]$, $[T_1]$, $[{}^1\text{O}_2]$, and $[\text{O}_2^-]$. The definitions for the photochemical parameters, ξ , β , η , δ , and σ , are shown in table 2, along with their relationships to the reaction rate constants.

The specific oxygen consumption rate, ξ , is the PDT oxygen consumption rate per light fluence rate and photosensitizer concentration under the condition that there is an infinite ${}^3\text{O}_2$ supply. σ , the specific photobleaching ratio, is the probability ratio of a ROS (including ${}^1\text{O}_2$ molecule) to react with ground state photosensitizer compared to the ROS (including ${}^1\text{O}_2$ molecule) reacting with a cellular target $[A]$. Notice that ξ and σ contains PDT photodynamic interaction from both type I and type II and are not separated. β represents the ratio of the monomolecular decay rate of the triplet state photosensitizer to the bimolecular rate of the triplet photosensitizer quenching by ${}^3\text{O}_2$ (Wang *et al* 2010) and is called the oxygen quenching threshold concentration (Zhu *et al* 2015a). η is the hypoxic consumption rate due to photobleaching reactions.

Table 2 also provides the definition of several other important photochemical parameters for a specific photosensitizer. Fluorescence quantum yield (Φ_{f}) of a compound is defined as the fraction of molecules that emit a photon after direct excitation (Demas and Crosby 1971). The triplet quantum yield (Φ_{t}) describes the crossover efficiency for PS to go from the singlet state to the triplet state via ISC (Bensasson *et al* 1972). Similarly, the singlet oxygen quantum yield (Φ_{Δ}) is given as the efficiency to produce singlet oxygen from the triplet state of a photosensitizer (Wilkinson *et al* 1993). We have introduced superoxide anion quantum yield (Φ_{ROS})

Table 2. Definition of some key parameters used in PDT modeling.

Symbol	Definition
β (μM)	Oxygen quenching threshold concentration $\frac{k_4 + k_8[A]}{k_2}$
δ (μM)	Low concentration correction
η ($\text{cm}^2 \text{mW}^{-1} \text{s}^{-1} \mu\text{M}$)	Hypoxic reaction consumption rate $\Phi_t \frac{\varepsilon}{h\nu} \frac{k_8[A]}{k_2}$
ξ ($\text{cm}^2 \text{mW}^{-1} \text{s}^{-1}$)	Specific oxygen consumption rate
σ (μM^{-1})	$\xi = \xi_{\text{II}} + \xi_{\text{I}} = S_{\Delta} \Phi_t \frac{\varepsilon}{h\nu} + S_{\text{I}} \Phi_t \frac{\varepsilon}{h\nu}$ Specific photobleaching ratio $\sigma = (\xi_{\text{II}} \sigma_{\text{II}} + \xi_{\text{I}} \sigma_{\text{I}}) / \xi$ where $\sigma_{\text{II}} = k_{12} \tau_{\Delta}$ and $\sigma_{\text{I}} = k_{11} \tau_{\text{S}}$
g ($\mu\text{M s}^{-1}$)	Macroscopic maximum oxygen supply rate
ε ($\text{cm}^{-1} \mu\text{M}^{-1}$)	Photosensitizer extinction coefficient
τ_{f} (s)	Fluorescence lifetime $\frac{1}{k_3 + k_5}$
τ_{Δ} (s)	Singlet oxygen lifetime $\frac{1}{k_{12}([S_0] + \delta) + k_6 + k_{72}[A]}$
τ_{S} (s)	Superoxide (ROS) lifetime $\frac{1}{k_{11}([S_0] + \delta) + k_{71}[A]}$
τ_{T} (s)	Triplet state lifetime $\frac{1}{k_4 + k_2[{}^3\text{O}_2] + k_8[A]}$
$[A]$ (μM)	Singlet oxygen receptors, considered a constant during PDT because it is too large to be changed during PDT.
S_{Δ}	Fraction of triplet-state photosensitizer- ${}^3\text{O}_2$ reactions to produce ${}^1\text{O}_2$
S_{I}	Fraction of triplet-state photosensitizer reactions involved in Type I reactions
S_{NL}	Fraction of triplet state photosensitizer reactions that are non-luminescent $S_{\Delta} + S_{\text{I}} + S_{\text{NL}} = 1$
Φ_{Δ}	Singlet oxygen quantum yield $S_{\Delta} \frac{k_5}{k_3 + k_5}$
Φ_{ROS}	Superoxide anion quantum yield $S_{\text{I}} \frac{k_5}{k_3 + k_5}$
Φ_{f}	Fluorescence quantum yield $\frac{k_5}{k_3 + k_5} \frac{k_{3\text{R}}}{k_3}$, where $k_{3\text{R}}$ is fluorescence radiative decay rate between S_1 and S_0
Φ_{t}	Triplet quantum yield $\frac{k_5}{k_3 + k_5}$

as the efficiency of producing superoxide anion from the triplet state of a photosensitizer. In addition to the quantum yields, the fluorescence lifetime (τ_{f}), triplet lifetime (τ_{T}), and singlet oxygen lifetime (τ_{Δ}) represent mean lifetime of each state (i.e. of the fluorescent state, the triplet state, and of singlet oxygen) (Strickler and Berg 1962). ε is the extinction coefficient ($\text{cm}^{-1} \mu\text{M}^{-1}$) defined as the absorption coefficient of the photosensitizer per concentration.

3.3. Relationship between rate parameters and the photochemical parameters

The rate constants for each of the reactions described previously can be determined by knowing some of the basic photochemical parameters mentioned before including the singlet oxygen lifetime (τ_{Δ}), the fluorescence lifetime (τ_{f}), the triplet lifetime (τ_{T}), and the triplet quantum yield (Φ_{t}), all of which are measurable quantities with existing technologies, which is described in section 4.

The photon absorption rate of the photosensitizer is given by knowing the extinction coefficient (ε) of the photosensitizer, the fluence rate ($\phi = 100 \text{ mW cm}^{-1}$), Planck's constant (h), and the frequency of light used for treatment (ν)

$$k_0 = \frac{\varepsilon\phi}{h\nu}. \quad (29)$$

The reaction rates involving $^1\text{O}_2$ (k_{12} , k_6 , k_7) can be determined by measuring the singlet oxygen lifetime. The relationship between τ_{Δ} and the rate constants is the following

$$\tau_{\Delta}^{-1} = k_{12}([S_0] + \delta) + k_6 + k_{72}[A]. \quad (30)$$

By varying the concentration of $[S_0]$ in water in the absence of any singlet oxygen acceptors ($[A] = 0$), the plot of τ_{Δ}^{-1} versus $[S_0]$ will yield a slope which will be k_{12} with a low concentration correction (δ) (Dysart and Patterson 2005, 2006). Furthermore the extrapolation to $[S_0] = 0$ will yield the value of k_6 , provided that the values of δ and k_{12} are known. Adding known concentrations of acceptors will allow for extrapolation of the value k_{72} . The value of δ can be found by investigating photobleaching kinetics and the steady-state singlet oxygen concentration approximation (Dysart *et al* 2005).

Triplet quantum yield (Φ_t) and fluorescence decay time (τ_f) can be used to calculate k_3 and k_5 with the following equations (Sternberg and van Gemert 1996)

$$\tau_f = \frac{1}{k_3 + k_5}, \quad (31)$$

$$k_3 = \frac{1 - \Phi_t}{\tau_f}, \quad (32)$$

$$k_5 = \frac{\Phi_t}{1 - \Phi_t} k_3 = \frac{\Phi_t}{\tau_f}. \quad (33)$$

Rate reactions involving the triplet state photosensitizer (k_2 , k_4 , k_8), are related to the triplet state lifetime by

$$\tau_t^{-1} = k_4 + k_2[{}^3\text{O}_2] + k_8[A]. \quad (34)$$

Measurement of the ground state oxygen in a phantom will enable extrapolation of k_2 and k_4 in a linear fit of τ_t^{-1} versus $[{}^3\text{O}_2]$ with the slope gives k_2 and extrapolation to $[{}^3\text{O}_2] = 0$ gives $k_4 + k_8[A]$. The oxygen quenching threshold concentration β ($= (k_4 + k_8[A])/k_2$) in the macroscopic model can be calculated with the ratio of the two. k_8 can be determined as the slope between τ_t^{-1} and $[A]$. All other photophysical parameters (ξ , σ , η) can be determined using the rate, k_i and the expression in table 2.

The quantum yield for generation of singlet oxygen (Φ_{Δ}) and superoxide anion (Φ_{ROS}) are important quantities in determining the concentrations of the cytotoxic oxygen species. Both are related to the photosensitizer triplet quantum yield by

$$\Phi_{\Delta} = S_{\Delta}\Phi_t, \quad (35)$$

$$\Phi_{\text{ROS}} = S_1\Phi_t. \quad (36)$$

4. Experimental methods to determine the rate parameters

The advent of spectroscopic techniques to measure rate constants of photosensitization and oxygenation has opened the way to the determination of their photochemical and photophysical parameters. This section describes a sampling of methods to determine experimental rate parameters and other key photochemical factors. The scope of this review is focused mainly on photochemical parameters *in vivo*. At present, this is only achievable through indirect methods (section 4.2)—namely extrapolation of the parameters in table 2 by applying the macroscopic model directly in *in vivo* systems. Most, if not all, of the direct methods to determine reaction rates are limited to *in vitro* systems or in phantoms. We will point out the potential for direct methods to *in vivo* system whenever possible. In addition, section 5 will point out the reaction rates that are inferred from *in vitro* measurements and are expected to remain the same *in vivo*.

4.1. Direct methods

4.1.1. Absorption spectroscopy. Absorption spectroscopy refers to a technique that measures the absorption of radiation by a sample. By using a spectrophotometer and a white light source, the extinction coefficient (ε ; units $\text{cm}^{-1} \mu\text{M}^{-1}$) of a photosensitizer can be determined by the Beer–Lambert law (Walsh 1955, Fuwa and Valle 1963)

$$A = -\ln \frac{I}{I_0} = \varepsilon lc, \quad (37)$$

where I is the output light intensity, I_0 is the input light intensity, l is the path length of the measured sample, and c is the concentration of the sample (in μM). Typically, absorbance, A , is defined for $l = 1$ cm). Notice our definition of extinction coefficient is \log_e based rather than \log_{10} based, the latter is often the case in the chemistry literature and cause ε to be decreased by a factor of 2.30 ($\ln 10$). Figure 7 shows an example of the wavelength dependence of ε , also called absorption spectra, for three PS (Photofrin, HPPH, and BPD). Using equation (29), the value of k_0 can easily be determined from the measured ε and knowing the measured wavelength, λ , of the light ($h\nu = hc \lambda^{-1}$).

Transient absorption spectroscopy. Transient absorption spectroscopy is an extension of absorption spectroscopy. Also called pump-probe spectroscopy, the absorbance of a sample is measured as a function of time after excitation by a flash of light, usually a pulsed laser, mainly to determine the triplet lifetime of the sensitizer, $[T_1]$ (Aveline *et al* 1998). This technique can be used to measure the singlet oxygen quantum yield (Φ_Δ) for a photosensitizer utilizing another chemical with known singlet oxygen quantum yields (Krieg and Redmond 1993, Krieg *et al* 1993).

4.1.2. Fluorescence spectroscopy. Photosensitizer fluorescence can be used to determine the concentration ($[S_0]$) of photosensitizer present both *in vivo* and *in vitro* (Konig *et al* 1993, Robinson *et al* 1998). However, fluorescence signal *in vivo* is affected by the tissue optical properties of scattering and absorption. The reduction of the fluorescence signal due to absorption can be accounted for by incorporating an empirical correction factor based on tissue optical properties (Finlay *et al* 2006). Many commonly used PS produce unique fluorescence spectra when excited at a certain wavelength. Figure 7 shows an example of three PS (Photofrin, HPPH, and BPD) and their fluorescence spectra. Such emission spectra, corrected for instrument response and tissue optical properties, can be analyzed as a linear combination of fluorescence basis spectra using a singular value decomposition (SVD) fitting algorithm (Finlay *et al* 2001). Fluorescence spectra from phantoms with known photosensitizer concentrations

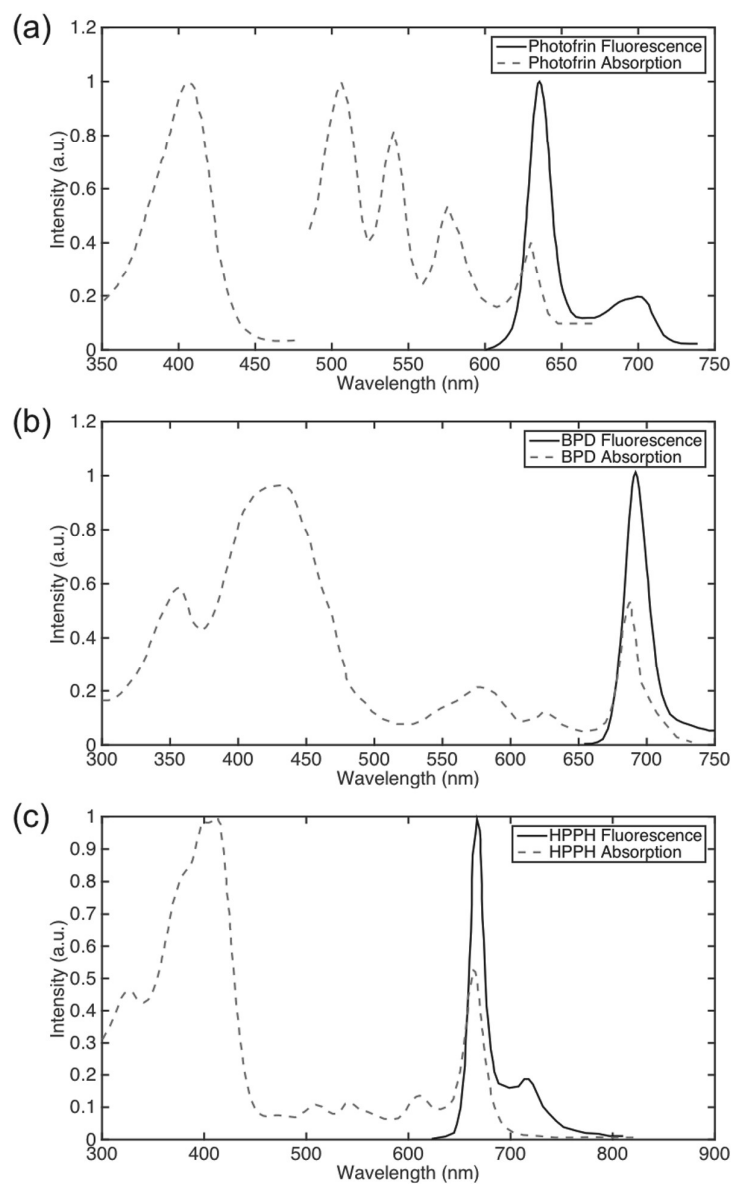


Figure 7. Fluorescence spectra (solid line) and absorption spectra (dashed line) of (a) Photofrin in PBS, (b) BPD in PBS, and (c) HPPH in water. Spectra are taken from Aveline *et al* (1994), Kim *et al* (2007), and Wezgowiec *et al* (2013) with permission. The absorption curve for (a) Photofrin above 480 nm has been multiplied by 10x for clarity.

can be used to determine the correction factor for fluorescence due to tissue optical properties as well as the absolute value of $[S_0]$ in an *in vivo* environment (Finlay *et al* 2006).

Fluorescence lifetime spectroscopy and imaging (FLI). Time-resolved fluorescence decay measurements can be used to study details about the structure and dynamics of macromolecules.

These measurements are commonly performed with microsecond to picosecond laser sources with high-speed photodetectors (Lakowicz *et al* 1992).

The fluorescence lifetime, τ_f , of PS can be determined from time-gated spectra along with single photon counting, using a picosecond to microsecond pulsed diode laser for fluorescence excitation. Specific wavelength ranges can be selected to plot the fluorescence exponential decay curve ($e^{-(k_3+k_5)t}$) to yield the decay constant ($k_3 + k_5$), which can be used to calculate $\tau_f = 1/(k_3 + k_5)$ (Kress *et al* 2003).

Laser-induced optoacoustic calorimetry (LIOAC). Triplet quantum yields, Φ_t , can be obtained by LIOAC and oxygen fluorescence quenching. After a laser pulsed excitation at the absorption wavelength (e.g. 532 nm) of the photosensitizer, radiationless relaxation processes of the intermediate states (e.g. S_1 , T_1 , ...) causes rapid deposition of heat in the sample, giving rise to acoustic waves, the magnitude of which are directly proportional to the heat evolved and can be detected by a piezoelectric transducer (Aveline *et al* 1994, Braslavsky and Heibel 1992). The absorbed energy deposited as heat in the sample within the detection window, αE_{abs} can be used to calculate the fluorescence and triplet quantum yield using (Aveline *et al* 1994)

$$(1 - \alpha)E_{\text{abs}} = \Phi_f E_s + \Phi_t E_t, \quad (38)$$

where E_s and E_t are the singlet state and triplet state energy gaps to the ground state, respectively. Experimentally, α is determined by comparing the calorimetric energy balance for the sample in question to an ideal reference system, which has a known $\alpha = 1$ (Aveline *et al* 1994).

4.1.3. Phosphorescence spectroscopy. Phosphorescence is similar to fluorescence in that absorbed energy by a substance is released in the form of light. However, phosphorescence occurs on a longer time scale than fluorescence. Besides the decays from monomol $^1\text{O}_2$ to $^3\text{O}_2 + h\nu$ at 1270 nm (22 kcal mol⁻¹), dimol singlet oxygen molecules ($2\ ^1\text{O}_2$) can also decay to 2 moles $^3\text{O}_2 + h\nu$ at 634 nm (44 kcal mol⁻¹) and 701 nm (Khan and Kasha 1963, 1964, 1970, Arnold *et al* 1964, 1965). The latter (634 nm and/or 701 nm) is readily observed in the gas phase but is often not detected in the solution due to other optical signals at these wavelengths. The detection of $^1\text{O}_2$ luminescence at 1270 nm is potentially difficult *in vivo* because of the short lifetime of $^1\text{O}_2$.

Singlet oxygen luminescence (SOL) detection (or laser flash photolysis). SOLD (or laser flash photolysis) is a standard technique for identification of short-lived, excited states of PS and characterization of their reactions (Krasnovskii 1976, Khan and Kasha 1979, Hurst *et al* 1982). It is a popular and precise technique used to directly measure k_6 and k_{72} , where the photosensitizer solution of the substrate is saturated with O_2 and irradiated with laser at a specific absorption wavelength. The resulting phosphorescence of $^1\text{O}_2$ at 1270 nm as a function of time is measured with a time-correlated detector (Kanofsky 1990). With the time-correlated single photon counting (TCSPC) module, phosphorescence decay characteristics can be measured with a time resolution of ≤ 100 ps and a spatial resolution in the subcellular region. With a high pulse repetition rate (40 MHz), the total acquisition time is short (less than 1 s) for each fluorescence decay curve (Kress *et al* 2003). Production of $^1\text{O}_2$ by laser excitation occurs in less than 2 μs , its decay is approximated by equations (39) and (40) (derived from equation (15)) and a first-order exponential decay of $^1\text{O}_2$ is given in equation (41). A Stern–Volmer plot of concentration of substrate $[A]$ versus $1/\tau_\Delta$ (where τ_Δ is the experimentally measured singlet oxygen lifetime), gives a straight line with the slope equal to k_{72} and the y-intercept equal to k_6

$$-\frac{d[^1\text{O}_2]}{dt} = \frac{1}{\tau_\Delta} [^1\text{O}_2] \quad (39)$$

$$[{}^1\text{O}_2] = [{}^1\text{O}_2]_0 e^{-t/\tau_\Delta} \quad (40)$$

$$\tau_\Delta^{-1} = k_6 + k_{72}[A] = k_d + (k_q + \gamma k_r)[A]. \quad (41)$$

The rate constants for oxidized product formation, k_r , are obtained by a competition technique reported by Higgins *et al* (1968) where the substrate solution containing photosensitizer and an alkene for comparative trapping to deduce the contribution from physical quenching k_q , can be obtained by difference using equation(41) (Clennan *et al* 1995, Celaje *et al* 2011). The variable γ in equation (41) is a function of the product chemical composition (see figure 6, $\gamma = 2$). Unlike unsaturated compounds such as alkenes, amines and polyenes are effective singlet oxygen physical quenchers and protect against photooxygenation (Wessels and Rodgers 1995).

Singlet oxygen quantum yields (Φ_Δ) can be determined from the phosphorescence intensity extrapolated back to zero time. These values can be recorded as a function of laser energy and of the absorbance for the sample and reference PS. Linear plots of the energy at each absorbance can be plotted (with the absorption factor) to produce slopes equivalent to the quantum yield (Marti *et al* 2000).

Measurement of this near-infrared (NIR) luminescence of singlet oxygen in biological environments is difficult due to the short ${}^1\text{O}_2$ lifetime (which can be less than the triplet-state PS lifetime) and its low quantum yield for phosphorescence. However, this can be achieved using a NIR-sensitive photomultiplier tube. Time-resolved analysis shows that ${}^1\text{O}_2$ lifetime is reduced ($\tau_\Delta = 0.03\text{--}0.18 \mu\text{s}$) *in vivo* compared to lifetime *in vitro* ($\tau_\Delta = 3.0 \pm 0.3 \mu\text{s}$). This may be due to the protein binding to ${}^1\text{O}_2$ in cellular environments (Niedre *et al* 2002). The photomultiplier tube must be sufficiently fast (with a rise time of ~ 3 ns) for phosphorescence single-photon counting, and it must have a broad, flat spectral response that enables spectral resolution of the ${}^1\text{O}_2$ signal (Jarvi *et al* 2006).

The shorter lifetime has been attributed to the rapid quenching of ${}^1\text{O}_2$ by biomolecules, combined with a lack of adequately sensitive detectors at NIR wavelengths, since the luminescence emission is proportional to the lifetime. When exchanging the H_2O solvent for D_2O , the lifetime of singlet oxygen increases by 20-fold. The τ_Δ in D_2O is $69 \mu\text{s}$ at 20°C and in H_2O $3.5 \mu\text{s}$ at 20°C (Ogilby and Foote 1983, Wilkinson *et al* 1993, Jensen *et al* 2010).

The triplet-state lifetime is highly dependent on the molecular oxygen concentration according to a Stern–Volmer relationship

$$\tau_t^{-1} = k_{4R} + k_{4NR} + k_2[{}^3\text{O}_2] = k_4 + k_2[{}^3\text{O}_2] \quad (42)$$

where k_{4R} and k_{4NR} are the radiative and nonradiative photosensitizer triplet state decay rate constants. The changes in triplet state lifetime (τ_t) can be used to determine changes in $[{}^3\text{O}_2]$, given k_2 and k_4 is known. In biological systems, $\tau_t \gg \tau_\Delta$ so that the exponential decay of the singlet oxygen luminescence curves is governed by τ_t (Shonat and Kight 2003, Poole *et al* 2004, Jarvi *et al* 2006).

Most singlet oxygen luminescence dosimetry (SOLD) studies have been done on microspheres of cells. Detection of SOL from a murine tumor using Photofrin and ATX-S10NAa(II) has been reported (Hirano *et al* 2002). The full luminescence spectrum can be measured by placing a monochromator in front of the detector.

The great impact of SOLD techniques comes with reports that show detection of ${}^1\text{O}_2$ in complex biological systems directly. The integrated detected ${}^1\text{O}_2$ luminescence counts is proportional to the total amount of ${}^1\text{O}_2$ created in the target during PDT and thus is predictive of PDT response (Jarvi *et al* 2006). Ultimately it is the cumulative ${}^1\text{O}_2$ dose that determines the biological effect. Furthermore, changes in the effective PDT dose due to oxygen depletion or due to photosensitizer photobleaching can be evaluated with time-resolved SOL measurements.

4.2. Indirect methods

Singlet oxygen explicit dosimetry (SOED) methods have been developed to calculate the reacted singlet oxygen, $^1[\text{O}_2]_{\text{rx}}$, *in vivo* and *in vitro* for type II PS. The main cytotoxic agent in type II PDT has been attributed to $^1\text{O}_2$ (Weishaupt *et al* 1976). PDT efficacy can be correlated to the calculated $^1[\text{O}_2]_{\text{rx}}$, thus making SOED an effective method of dosimetry for *in vivo* studies as well as in clinical settings. The methodology for SOED for type II photosensitizer can be expanded for ROS involving type I PS, even though it has not been used in existing studies. However, the parameters obtained should include photodynamic action from both type I and type II even though singlet oxygen is predominant for the type II PS studied.

4.2.1. SOED *in vitro* and in phantoms. SOED methods have been used *in vitro* to determine photochemical parameters in table 2 (β , δ , ξ , and σ) (Patterson *et al* 1990, Foster *et al* 1991, 1993, Nichols and Foster 1994, Georgakoudi *et al* 1997, Dysart and Patterson 2006). Spheroids of cell have been used to model PDT-induced oxygen depletion using equations very similar to those of section 3.2. Cell suspensions in cuvettes have been irradiated to investigate PDT *in vitro* and light fluence dependent effects (Sporn and Foster 1992). Cell survival assays are used as an endpoint to assess fluorescence-based singlet oxygen dose metrics (Dysart and Patterson 2006). In phantoms, singlet oxygen can be trapped by various compounds and thus detected indirectly. Most common compounds for $^1\text{O}_2$ are SOSG and MNR as described in section 4.3.

Spheroid cell survival assays have been used to determine the threshold dose of singlet oxygen for necrosis as well as photochemical parameters (β , δ , ξ , and σ) (Foster *et al* 1993, Georgakoudi *et al* 1997). Monolayers of cell cultures are initiated into spheroids $\sim 500 \mu\text{m}$ in diameter. Treated spheroids are dissociated and the fraction of cells that survive treatment is determined by a colony formation assay (Foster *et al* 1993, Georgakoudi *et al* 1997). An expression that relates the experimentally determined spheroid cell surviving fraction to the total rate of oxygen consumption (the sum of both metabolic oxygen consumption rate, which is assumed to be unaffected by PDT, and the oxygen consumption rate due to PDT processes) is used to determine a coefficient of PDT-induced oxygen consumption. Furthermore, a threshold dose of $^1\text{O}_2$ can be determined for cell spheroids, where once this dose has been delivered to the cells within the spheroid shell and $^3\text{O}_2$ has been depleted, continued irradiation at the same fluence rate will not result in significant additional cell killing (Foster *et al* 1993). Measurements of $^3\text{O}_2$ depletion and a knowledge of $^3\text{O}_2$ diffusion in cells and consumption due to PDT can be used to describe $^3\text{O}_2$ transport in a cell spheroid system. This can further be used to calculate the amount and distribution of $^1\text{O}_2$ molecules in a multicell-spheroid model during PDT (Nichols and Foster 1994).

Oxygen consumption and photobleaching studies with spheroids cells have been used to determine the probability of $^1\text{O}_2$ reaction with ground state photosensitizer, σ ($k_1/k_7[A]$) as well as the ratio of k_4/k_2 (β). Using measurements from oxygen microelectrodes, the following equation for oxygen consumption was fit to determine σ (Georgakoudi *et al* 1997, Georgakoudi and Foster 1998)

$$\frac{d[{}^3\text{O}_2]}{dt}(t) = \xi[S_0]_0\phi \left(\frac{[{}^3\text{O}_2](t)}{[{}^3\text{O}_2](t) + \beta} \right) \exp\left(-\sigma \int_0^t \frac{d[{}^3\text{O}_2]}{dt}(t') dt' \right). \quad (43)$$

The left hand side of equation (43) is the rate of photodynamic oxygen consumption and $\xi[S_0]_0\phi$ is the maximum or initial rate of photodynamic oxygen consumption. In this spheroid model, the oxygen perfusion rate (g) present in equation (25) is set to 0 since no vasculature is present. Georgakoudi *et al* found that σ is $90 \pm 15.9 \text{ M}^{-1}$ for ALA-induced PpIX

photobleaching and $76 \pm 12 \text{ M}^{-1}$ for Photofrin (Georgakoudi *et al* 1997) assuming a uniform distribution of photosensitizer. Spheroid cells and oxygen microelectrode measurements have also been used to investigate β . Mitra *et al* have found that β is $8.7 \pm 2.9 \mu\text{M}$ for mTHPC-mediated PDT and σ is $29.7 \pm 4.6 \text{ M}^{-1}$ (Mitra and Foster 2005). Reanalysis of Photofrin data with the observation of Photofrin's nonuniform distribution yielded values of $\beta = 12.1 \pm 3.4 \mu\text{M}$ and $\sigma = 56.5 \pm 8.6 \text{ M}^{-1}$ (Mitra and Foster 2005), which is not remarkably different from $\beta = 11.9 \pm 2.2 \mu\text{M}$ as determined with an assumed uniform distribution of Photofrin (Georgakoudi *et al* 1997). The threshold dose of $^1\text{O}_2$ in spheroid cells using Photofrin-mediated PDT was found to be $11.9 \pm 3.5 \text{ mM}$ (Mitra and Foster 2005).

4.2.2. SOED *in vivo*. For SOED, it is critical to know the photochemical parameters, (β , ξ , σ , δ , and g), and the singlet oxygen threshold dose, $[^1\text{O}_2]_{\text{rx,sh}}$. These parameters can be determined by performing PDT on a mouse model (Wang *et al* 2010, Liang *et al* 2012, Liu *et al* 2013, 2014, McMillan *et al* 2013, Zhu and Liu 2013, Kim *et al* 2014a, 2016, 2015, Zhu *et al* 2014, 2007, 2015a, Penjweini *et al* 2015a). Tumors are grown on mice and after injection with photosensitizer, treatment is delivered interstitially using a cylindrically diffusing fiber inserted inside the tumor. Partial treatment of the tumor is performed using various light doses and fluence rates. After treatment, the tumors are sectioned perpendicular to the linear treatment and stained with hematoxylin and eosin (*H & E*) to assess the necrotic area. Necrotic area is then used to calculate necrosis radius ($A = \pi r^2$, where A is the area and r is the necrosis radius). PDT-induced necrosis is determined by subtracting the radius of necrosis from control mice with no PDT treatment. Necrosis radius is then used with the spatially- and temporally-resolved calculated $^1[\text{O}_2]_{\text{rx}}$ profile using the macroscopic model equations from section 3.2. Experimentally obtained data is used for the model equations. Light fluence distribution inside the tumor is calculated by measuring the absorption and scattering optical properties (μ_a and μ'_s) (Zhu *et al* 2005). Photosensitizer concentration inside the tumor is determined using fluorescence spectra that are corrected for optical property effect (Finlay *et al* 2001). The correction factor is determined prior to experimentation in phantom studies with known photosensitizer concentrations and varying optical properties (Kim *et al* 2014a, 2015).

The model parameters are then varied globally so that the $[^1\text{O}_2]_{\text{rx}}$ for each mouse at the necrosis radius is close to the 'apparent $[^1\text{O}_2]_{\text{rx,sh}}$ '. This quantity is then the singlet oxygen threshold dose. An initial guess for these model parameters must be provided for the fitting routine. Initial *in vivo* model parameters have been published previously (Zhu *et al* 2007, 2014, 2015a, Wang *et al* 2010, Liang *et al* 2012, Liu *et al* 2013, 2014, McMillan *et al* 2013, Zhu and Liu 2013, Kim *et al* 2014a, 2016, 2015; Penjweini *et al* 2015a). Threshold singlet oxygen doses ($[^1\text{O}_2]_{\text{rx,sh}}$) *in vivo* using mouse models were fitted to be $0.56 \pm 0.26 \text{ mM}$, $0.72 \pm 0.21 \text{ mM}$, and $0.60 \pm 0.18 \text{ mM}$ for Photofrin, BPD, and HPPH respectively (Wang *et al* 2010, McMillan *et al* 2013, Kim *et al* 2014a, 2016, 2015, Liu *et al* 2014, Zhu *et al* 2015a). The other parameters are summarized in table 5.

4.3. Other methods

In addition to the experimental methods mentioned in this section, there are other techniques that can be used to investigate the presence of the reactive oxygen species. These methods have been mostly used *in vitro*; however, some may be applicable in *in vivo* systems as well. These methods involve fluorescent markers and analytical methods.

Several methods are developed to detect the presence of singlet oxygen and/or HO^\bullet . Singlet oxygen can be detected from dioxetanes from [2 + 2] cycloadditions, endoperoxides from [2 + 4] cycloadditions, and allylic hydroperoxides from 'ene' reactions (Clennan and Foote

1992, Aubry *et al* 2003). Simple alkenes often take up 1 equivalent of $^1\text{O}_2$. Tandem $^1\text{O}_2$ reactions can take place in polyunsaturated compound, there are also instances where bisperoxides rearrange to spiro compounds. Peroxides can also be generated through type I reaction that do not involve singlet oxygen, for example, there are electron transfer photooxidation reactions with 9-mesityl-10-methylacridinium ion (Kotani *et al* 2004, Ohkubo *et al* 2005). It may be noted that ene-derived hydroperoxides and cycloaddition-derived endoperoxides have a toxicity of their own that is separate of singlet oxygen's toxicity (Ouedraogo and Redmond 2003, Chakraborty *et al* 2009).

Aromatic compounds such as 9,10-disubstituted anthracenes can trap $^1\text{O}_2$ and be detected by UV–vis spectroscopy (Ragas *et al* 2009, Kim *et al* 2014b, Pedersen *et al* 2014). Another trapping reaction is 9,10-anthracene-9,10-endoperoxide dipropionate dianion that arises from a [2 + 4] cycloaddition of $^1\text{O}_2$ with 9,10-anthracene dipropionate dianion at pH = 10 in water detected by UV–visible spectroscopy.

Analytical methods such as low-temperature NMR spectroscopy can be used to detect unstable peroxide compounds in reaction mixtures. For example, dioxetane ^{13}C NMR signals are fairly characteristic (Baumstark 1988). Electron-rich olefins such as alkoxy-substituted alkenes react with singlet oxygen and form dioxetanes. Decomposition of dioxetanes is often accompanied by chemiluminescence due to a fragmented excited carbonyl compound (Adam and Trofimov 2006, Turro *et al* 2010).

Singlet oxygen sensor green (SOSG) is a $^1\text{O}_2$ -specific fluorescent probe reagent that has been used to quantitatively measure $^1\text{O}_2$ that has been produced by determining the reaction rate of SOSG with $^1\text{O}_2$. SOSG is a fluorescein–anthracene dye that fluoresces after its reaction with $^1\text{O}_2$. The endoperoxide product from a [2 + 4] cycloaddition of $^1\text{O}_2$ closes off the FRET quenching channel of precursor SOSG (Ragas *et al* 2009, Gollmer *et al* 2011). SOSG reacts with $^1\text{O}_2$ to produce SOSG endoperoxides, which emits a strong fluorescence signal at 531 nm. Φ_Δ has also been determined using SOSG for a porphyrin-based photosensitizer, hematoporphyrin monomethyl ether (Lin *et al* 2013).

Fluorescence probes can also be used to detect highly ROS such as hydroxyl radical (HO^\bullet) and reactive intermediates of peroxidase. 2-[6-(4'-hydroxy)phenoxy-3H-xanthen-3-on-9-yl] benzoic acid (HPF) and 2-[6-(4'-amino)phenoxy-3H-xanthen-3-on-9-yl]benzoic acid (APF) are two examples of such fluorescent probes (Setsukinai *et al* 2003). Both probes are reported to be cell-permeable, relatively insensitive to superoxide anion, nitric oxide, $^1\text{O}_2$, and alkyl peroxides (Price *et al* 2009, Price *et al* 2013). APF is ~5 times more fluorescent during HO^\bullet formation than HPF (Price *et al* 2009). Other fluorescent probes of hydroxyl radical include coumarin- and rhodamine nitroxide-based compounds (Yuan *et al* 2010, Yapici *et al* 2012, Meng *et al* 2014).

Table 3 summarizes all methods available to determine rate constants and other photochemical parameters, along with whether or not the technique has been applied in an *in vivo* model. The methods mentioned in this section can be useful tools to determine *in vivo* and *in vitro* photochemical parameters as well as characteristics of reactive species relevant for a specific photosensitizer. Based on this review, we consider the technique for fluorescence and SOLD-based lifetime (τ_f , τ_t , τ_Δ) measurements to be mature and able to accurately determine rate constants (k_1 , k_2 , $k_3 + k_5$, k_4 , k_6 , k_7) as described in section 3.3. To determine k_3 and k_5 , it is important to determine the triplet quantum yield, Φ_t , which can be determined using LIOAC. We also consider absorption measurements to be very mature and accurately determines the extinction coefficient ε and k_0 . However, the technique to determine the singlet oxygen quantum yield, Φ_Δ , is still dependent on the known reference singlet oxygen quantum yield, and thus may contain errors. Only indirect methods are available to determine Φ_Δ value *in vivo*, which can be substantially different from the *in vitro* value.

Table 3. Summary of the experimental methods described in this section.

Method		References
Direct methods	Continuous wave / Transient/lifetime	
Absorption	Absorption spectroscopy (k_0, ε) (<i>in vivo/in vitro</i>)	Walsh (1955), Fuwa and Valle (1963), Chattopadhyay <i>et al</i> (1984), Krieg and Redmond (1993), Krieg <i>et al</i> (1993) and Aveline <i>et al</i> (1998)
Fluorescence	Fluorescence spectroscopy ($[S_0]$) (<i>in vivo/in vitro</i>)	Lakowicz <i>et al</i> (1992), Finlay <i>et al</i> (2001) and Kress <i>et al</i> (2003)
Phosphorescence	LIOAC (Φ_t)	Aveline <i>et al</i> (1994)
	Phosphorescence spectroscopy	SOL detection ($\tau_t, \tau_\Delta, k_1, k_2, k_4, k_6, k_7$) (<i>in vitro</i> mostly) phosphorescence spectroscopy ($[^3O_2]$) (<i>in vivo/in vitro</i>)
Indirect methods		
SOED	<i>In vitro</i> studies ($\xi, \sigma, \beta, \delta$)	Patterson <i>et al</i> (1990), Foster <i>et al</i> (1991, 1993), Nichols and Foster (1994), Georgakoudi <i>et al</i> (1997) and Dysart and Patterson (2006)
	<i>In vivo</i> studies ($\xi, \sigma, \beta, \delta, g$)	Zhu <i>et al</i> (2007, 2014, 2015a), Wang <i>et al</i> (2010), Liang <i>et al</i> (2012), Liu <i>et al</i> (2013, 2014), McMillan <i>et al</i> (2013), Zhu and Liu (2013), Kim <i>et al</i> (2014a, 2016, 2015) and Penjweini <i>et al</i> (2015a)
Other methods		
	Singlet oxygen trapping ($[^1O_2]$)	Kotani <i>et al</i> (2004), Ohkubo <i>et al</i> (2005), Ragas <i>et al</i> (2009), Pedersen <i>et al</i> (2014) and Kim <i>et al</i> (2014b)
	NMR spectroscopy ($[^1O_2]$)	Baumstark (1988)
	SOSG ($[^1O_2], \Phi_\Delta$)	Lin <i>et al</i> (2013)
	APF, HPF ($[HO^\bullet]$)	Setsukinai <i>et al</i> (2003)

5. A review of existing values of photochemical parameters

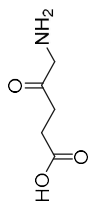
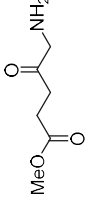
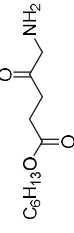
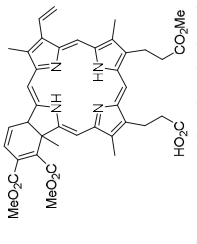
PS are normally delivered systemically or topically in PDT. The systemic administration involves either oral administration or intravenous injection so that the drug will be circulated through the whole body system, and preferentially more drug will be localized in the target site than in others. An ideal photosensitizer should have low or no toxicities and a fast clearance process. Some systemically delivered PS are benzoporphyrin derivative (BPD), Photofrin, and HPPH (2-[1-hexyloxyethyl]-2-devinyl pyropheophorbide-a). In contrast with the systemic administration, ALA, a pro-drug that reacts with heme to generate the photosensitizer protoporphyrin IX (PpIX), can also be applied topically to perform more localized delivery, which is commonly used for skin treatment. Table 4 summarizes common PS that are currently used in various stages of clinical trials. Note that most of the PS are of type II category, with the exception of Tookad (WST-09) and WST-11, which are type I PS (Vakrat-Haglili *et al* 2005, Ashur *et al* 2009).

There are several PS that have been approved for standard clinical use by the US Food and Drug Administration (FDA) or the European Medicines Agency (EMA) (Huang 2005, Agostinis *et al* 2011). ALA (a pro-drug that produces PpIX) was approved for the treatment of actinic keratoses in 1999 by the FDA under the trade name Levulan (Jeffes 2002) and in 2009 and 2011 by the EMA under the trade name Alacare and Ameluz, respectively. Similar photosensitizer derivatives were developed to also produce PpIX: methyl-ALA was approved by the FDA in 2004 for the treatment of non-hyperkeratotic actinic keratoses, and hexyl-ALA was approved in Europe in 2006 for the diagnosis of bladder cancer under the trade name Hexvix (Lapini *et al* 2012). In 2000, the FDA approved use of BPD in the treatment of age-related macular degeneration (Mody 2000). mTHPC was approved by the EMA for treatment of head and neck squamous cell carcinomas. Photofrin was approved by the FDA for multiple treatment sites. It was approved for microinvasive endobronchial non-small cell lung cancer in 1998 and high-grade dysplasia in Barrett's esophagus in 2003.

The photochemical parameters, β , δ , ξ , σ , and g , can be determined using indirect methods mentioned previously (table 3) (Mitra and Foster 2005, Wang *et al* 2010, Liu *et al* 2013). Currently only a subset of PS in table 5 (Photofrin, ALA, BPD, HPPH, mTHPC) have been studied. Every photosensitizer should undergo studies to determine the photochemical parameters so that they may be used for modeling the PDT process as well as dosimetry. The fundamental photophysical parameters of most, if not all, PS are fairly well established (e.g. ϵ , τ_f , τ_T), and they can be used to determine some parameters, such as ξ , for PS. However, indirect methods *in vivo* can only be used to determine the ratios of rate constants (k_i 's, where $i = 1-8$), thus additional measurements are necessary to determine individual reaction rate constants. In this review, all parameters were determined for FDA or EMA approved PS (table 5(a)) as well as some others (table 5(b)). Table 5 summarizes the known values and references for the PS listed in table 4. Notice that this is a very incomplete list and includes only the most commonly and clinically used PS.

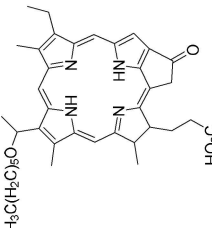
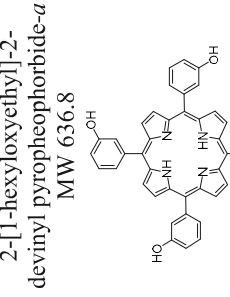
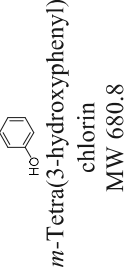
The photochemical parameters for most PS were determined *in vitro*. However, it is reasonable to expect that they will largely remain the same in *in vivo* systems (such as ϵ , k_0 , k_3 , and k_5). Thus, their values can be determined *in vitro* or *in vivo* for most PS. Some of the parameters (k_6 , k_{72}) are photosensitizer independent since they are properties of either $^1\text{O}_2$ or other ROS and they should behave the same. Assumptions can be made that they are the same for all type II PS. Two of the PS summarized in this review are of type I, but it can be assumed that the

Table 4. Characteristics of common PS and their FDA or EMA status.

Photosensitizer (trade name)	Chemical structure	Approval	λ_{ex} (nm)	DLI ^a (h)	Clearance time	References
ALA-PpIX (Levulan, Alacare, Ameluz, Gliolan (for photodiagnosis))	 5-aminolevulinic acid MW 131.1	1999 (FDA) 2009 2011 2007 (EMA)	405, 635	14–18	~2 d	Ericson <i>et al</i> (2004), Hage <i>et al</i> (2004), Kely <i>et al</i> (2004) and Touma <i>et al</i> (2004)
Methyl ALA-PpIX (Medvix, Metvixia)	 methyl aminolevulinatate MW 145.2	2004 (FDA)	405, 635	3	~2 d	Dragieva <i>et al</i> (2004)
Hexyl ALA-PpIX (Hexvix)	 hexyl-5-aminolevulinatate MW 215.3	2000 (FDA)	689	0.25–3	5 d	Momma <i>et al</i> (1998), Lui <i>et al</i> (2004), Azab <i>et al</i> (2005) and Chen <i>et al</i> (2005)
BPD-MA (Verteporfin, Visudyne)	 benzoporphyrin derivative monoacid ring A MW 718.8					

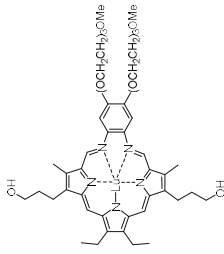
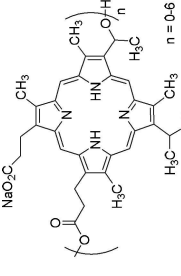
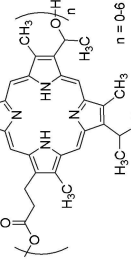
(Continued)

Table 4. (Continued)

Photosensitizer (trade name)	Chemical structure	Approval	λ_{ex} (nm)	DLI ^a (h)	Clearance time	References
HPPH	 <p>H₃C(H₂O)₅O</p>		665	24	~3 d	Bellnier <i>et al</i> (2003)
mTHPC (Foscan)	 <p>2-[1-hexyloxyethyl]-2-devinyl pyropheophorbide-a MW 636.8</p>	2001 (EMA)	652	48–110	15 d	Verigos <i>et al</i> (2006)
	 <p><i>m</i>-Tetra(3-hydroxyphenyl)chlorin MW 680.8</p>					

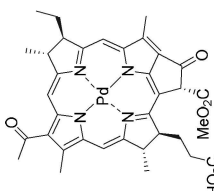
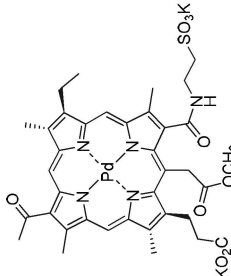
(Continued)

Table 4. (Continued)

Photosensitizer (trade name)	Chemical structure	Approval	λ_{ex} (nm)	DLI ^a (h)	Clearance time	References
mLu (Lu-Tex)			732	3	~2 d	Stripp <i>et al</i> (2004) and Verigos <i>et al</i> (2006)
Porfimer sodium (Photofrin)	 MW 1169.1	1998, 2003 (FDA) 2004 (EMA)	630	48–150	4–6 weeks	Arnfield <i>et al</i> (1993), Chen <i>et al</i> (1997), Lee <i>et al</i> (1997), Marks <i>et al</i> (2000), Wiedmann <i>et al</i> (2003, 2004), Cuenca <i>et al</i> (2004) and Igbasemokumo (2004),
	 MW 605.7					

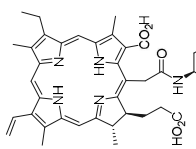
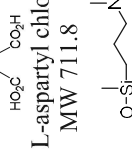
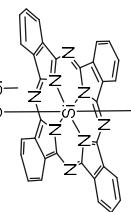
(Continued)

Table 4. (Continued)

Photosensitizer (trade name)	Chemical structure	Approval	λ_{ex} (nm)	DLI ^a (h)	Clearance time	References
WST09 (Tookad)	 <p>palladium-metallated bacteriopheophorbide MW 714</p>		763	~0.1–0.25	~2 h	Weersink <i>et al</i> (2005a, 2005b)
WST11	 <p>Palladium bacteriochlorin 130-(2-sulfoethyl) amide dipotassium salt MW 940</p>		760	~0.1–0.25	~1 h	Mazor <i>et al</i> (2005)

(Continued)

Table 4. (Continued)

Photosensitizer (trade name)	Chemical structure	Approval	λ_{ex} (nm)	DLI ^a (h)	Clearance time	References
Talaporfin sodium (LS11)			664	1	14 d	Spikes and Bommer (1993a), Kato <i>et al</i> (2003) and Lustig <i>et al</i> (2003)
Pc-4	mono-L-aspartyl chlorin <i>e</i> ₆ MW 711.8 		672	24–36	~28 h	Miller <i>et al</i> (2007), Baron <i>et al</i> (2010) and Kinsella <i>et al</i> (2011)
	silicon phthalocyanine MW 719.94 					

^aDLI: drug-light interval.

corresponding parameters (k_6, k_{71}, k_8) are dependent only on the microenvironment and thus are approximately the same for different type I PS. Some photochemical parameters (k_1, k_2, k_4) are more environmentally dependent. Therefore it can be expected that the values for such parameters would be different between *in vivo* and *in vitro* conditions. One reason for this difference is due to aggregation which leads to photosensitizer–photosensitizer photoreactions. It was found that the ratio β was roughly the same for all PS, which can help to estimate this value for unknown PS (Mitra and Foster 2005).

This review of photochemical parameters indicates that some of the k_i 's (k_2, k_4, k_6, k_7) are roughly of the same order of magnitude for all PS. Some of the k_i 's (k_3, k_5) are the same order of magnitude for all type I or type II PS, but otherwise differ between the two types. Thus we believe they can be used to identify whether a particular photosensitizer will have type I or type II tendencies.

There are quite a number of photochemical parameters that are still unknown (see table 5 for values either missing ('—') or estimated in parenthesis). Further studies are necessary to determine these values *in vivo* directly. It is possible to expand the technology for direct method (table 3) to be used *in vivo*.

For BPD, the extinction coefficient (ε) was found to be $0.0783 \text{ cm}^{-1} \mu\text{M}^{-1}$ using absorption spectroscopy (Aveline *et al* 1994, Zhu *et al* 2014). The value of k_0 was found at a fluence of 100 mW cm^{-2} using equation (29) and ε . k_{12} was found by using the approximation $k_{12} \approx \sigma_{\text{II}} \cdot k_{72}[A]$, where σ_{II} is the specific photobleaching ratio determined *in vivo* using SOED in section 4.2.2. k_2 was found to be $3 \times 10^3 \mu\text{M}^{-1} \text{ s}^{-1}$ using the observed triplet lifetime (τ_t) in the presence and absence of $^3\text{O}_2$ (equation (34)) (Aveline *et al* 1994). Using this value, and the measured value for β *in vivo*, k_4 can be found to be $k_4 = \beta \times k_2 = (11.9 \mu\text{M}) \times (3 \times 10^3 \mu\text{M}^{-1} \text{ s}^{-1}) = 3.6 \times 10^4 \text{ s}^{-1}$. The values for k_3 and k_5 were found by using the fluorescence lifetime (τ_f) and the triplet quantum yield (Φ_t) and equations (31)–(33). The value of τ_f was taken from literature Aveline *et al* using a time-correlated single photon counting method (Aveline *et al* 1994). The value of Φ_t was obtained from literature using LIOAC (see table 3 and section 4) (Aveline *et al* 1994). The resulting values were $k_3 = (1 - \Phi_t)/\tau_f = (1 - 0.79)/(5.2 \times 10^{-9} \text{ s}) = 4.04 \times 10^7 \text{ s}^{-1}$ and $k_5 = \Phi_t/\tau_f = 0.79/5.2 \times 10^{-9} \text{ s} = 1.52 \times 10^7 \text{ s}^{-1}$. The singlet oxygen lifetime (τ_Δ) in water with no acceptors to react with $^1\text{O}_2$ can be used with equation (30) to obtain the value of k_6 , which is only a property of singlet oxygen and should be photosensitizer independent. Therefore, for all type II PS, $k_6 = \tau_\Delta^{-1} = (3 \mu\text{s})^{-1} = 3.3 \times 10^5 \text{ s}^{-1}$ (Zhu *et al* 2015a). The value of $k_{72}[A]$ *in vivo* is only a property of singlet oxygen and is thus assumed to be the same for all type II PS. By using the value of τ_Δ in tissue ($0.1 \mu\text{s}$) and the known value for k_6 , $k_{72} = \tau_\Delta^{-1} - k_6 = (0.1 \mu\text{s})^{-1} - (3.3 \times 10^5 \text{ s}^{-1}) = 1 \times 10^7 \text{ s}^{-1}$ (Dysart *et al* 2005). Since BPD is a type II photosensitizer, there is no significant contribution of type I reactions between $[T_1]$ and $[A]$ so $k_8[A]$ and η were assumed to be 0. The values of ξ , σ , and g were found *in vivo* using the SOED method (McMillan *et al* 2013, Kim *et al* 2014a, 2016, Zhu *et al* 2015a). Details for the SOED method are in section 4.2.2. The low concentration correction, δ , was assumed to be the same for BPD as that of Photofrin. Further experiments are needed to confirm this value for BPD. The fraction of $^1\text{O}_2$ producing reactions between $[T_1]$ and $^3\text{O}_2$ was determined using the definition of ξ in table 2: $S_\Delta = \xi/\Phi_t/\varepsilon \times (h\nu) = (51 \times 10^{-3} \text{ cm}^2 \text{ mW}^{-1} \text{ s}^{-1})/(0.79)/(0.0312 \mu\text{M}^{-1} \text{ cm}^{-1}) \times (6.022 \times 10^{14} \text{ cm}^3 \mu\text{M}^{-1}) \times (2.72 \times 10^{-16} \text{ mW s}) = 0.144$.

Table 5. Clinically relevant photosensitizers and their photophysical parameters.

Parameter	ALA-PpIX	BPD	mTHPC	Photofrin
ϵ ($\text{cm}^{-1} \mu\text{M}^{-1}$)	0.003 @633 nm (Lovell <i>et al</i> 2010, Liu <i>et al</i> 2012)	0.0783 @690 nm (Aveline <i>et al</i> 1994, Zhu <i>et al</i> 2014)	0.111 @650 nm (Johansson <i>et al</i> 2006)	0.0035 @630 nm (Bonnet <i>et al</i> 1983, Zhu <i>et al</i> 2014)
k_0 @100 mW cm^{-2} (s^{-1})	1.59 ^a	45.13 ^a	60.27 ^a	1.84 ^a
k_1 ($\mu\text{M}^{-1} \text{s}^{-1}$)	9×10^{2b} (0.85–900) (Cox and Whitten 1982, Georgakoudi and Foster 1998)	1.7×10^{2b} (150–550) (McMillan <i>et al</i> 2013, Kim <i>et al</i> 2014a)	2.97×10^{2b} 12–297 (Dysart <i>et al</i> 2005, Mitra and Foster 2005)	7.6×10^{2b} (Georgakoudi <i>et al</i> 1997)
k_2 ($\mu\text{M}^{-1} \text{s}^{-1}$)	1.9×10^3 (1700–2100) (Jarvi <i>et al</i> 2011)	3×10^3 (Aveline <i>et al</i> 1994)	2.6×10^3 (2500–2700) (Jarvi <i>et al</i> 2011)	1.4×10^3 (Sternborg and van Gemert 1996)
k_3 (s^{-1})	2.9×10^{7c} (Sternborg and van Gemert 1996)	4.04×10^{7d} (Aveline <i>et al</i> 1994)	1.47×10^{7d}	2.9×10^7 (Sternborg and van Gemert 1996)
k_4 (s^{-1})	2.3×10^{4e} (3.5×10^3 – 2.3×10^4)	3.6×10^{4e}	2.3×10^{4e} (0.9×10^4 – 2.3×10^4)	1.67×10^{4e}
k_5 (s^{-1})	1.2×10^{7f}	1.52×10^{7f}	1.19×10^{8f}	4.94×10^{7f}
k_6 (s^{-1})	3.3×10^{5g}	3.3×10^{5g}	3.3×10^{5g}	3.3×10^{5g}
$k_7[A]$ (s^{-1})	1×10^{7h} (3×10^6 – 3×10^7)	1×10^{7h} (3×10^6 – 3×10^7)	1×10^{7h} (3×10^6 – 3×10^7)	1×10^{7h} (3×10^6 – 3×10^7)
$k_8[A]$ (s^{-1})	(0) ^j	(0) ^j	(0) ^j	(0) ^j
β (μM)	(11.9) ^c	(11.9) ^c	8.7 (Mitra and Foster 2005)	11.9 (Georgakoudi <i>et al</i> 1997)
δ (μM)	(33) ^c (33–150) (Dysart <i>et al</i> 2005, Liu <i>et al</i> 2012)	(33) ^c (33–260) (Weston and Patterson 2011)	(33) ^c (33–150) (Mitra and Foster 2005)	33 (33–150) (Dysart <i>et al</i> 2005)

(Continued)

Table 5. (Continued)

Parameter	ALA-PpIX	BPD	mTHPC	Photofrin
ξ ($\text{cm}^2 \text{mW}^{-1} \text{s}^{-1}$)	3.7×10^{-5c}	$(51 \pm 15) \times 10^{-3}$ (McMillan <i>et al</i> 2013, Kim <i>et al</i> 2014a)	30×10^{-3} (Mitra and Foster 2005, Zhu <i>et al</i> 2015a)	3.7×10^{-3} ($2.9\text{--}3.7$) $\times 10^{-3}$ (Georgakoudi <i>et al</i> 1997, Mitra and Foster 2005, Zhu <i>et al</i> 2014)
σ (μM^{-1})	$(9.0 \pm 1.6) \times 10^{-5}$ ($2.8 \times 10^{-8}\text{--}9 \times 10^{-5}$) ⁱ (Georgakoudi and Foster 1998, Zhu <i>et al</i> 2015a)	1.7×10^{-5} ($(1\text{--}5) \times 10^{-5}$) (McMillan <i>et al</i> 2013, Kim <i>et al</i> 2014a)	$(2.97 \pm 0.46) \times 10^{-5}$ ($1.2\text{--}1.7$) $\times 10^{-6}$ (Mitra and Foster 2005, Zhu <i>et al</i> 2015a)	7.6×10^{-5} (Georgakoudi <i>et al</i> 1997)
η ($\text{cm}^2 \text{mW}^{-1} \text{s}^{-1} \mu\text{M}$)	(0) ⁱ	(0) ⁱ	(0) ⁱ	(0) ⁱ
g ($\mu\text{M s}^{-1}$)	—	1.7 ± 0.7^k (McMillan <i>et al</i> 2013, Kim <i>et al</i> 2014a)	—	0.76 (Wang <i>et al</i> 2010)
S_Δ	0.281 ^j	0.144 ^j	0.104 ^j	0.319 ^j
Φ_t	0.83 (Josefsen and Boyle 2008)	0.79 (Aveline <i>et al</i> 1994)	0.89 (Mitra and Foster 2005)	0.63 (0.63–0.80) (Foster <i>et al</i> 1991, Mitra and Foster 2005, Zhu <i>et al</i> 2014)
Φ_Δ	0.233 ^k (0.54–0.77) (Cox <i>et al</i> 1982, Redmond and Gamlin 1999)	0.114 ^k (0.17–0.84) (Fernandez <i>et al</i> 1997, Redmond and Gamlin 1999)	0.093 ^k (0.3–0.43) (Hadjur <i>et al</i> 1998, Dysart <i>et al</i> 2005)	0.20 ^k (0.12–0.56) (Mitra and Foster 2005, Lovell <i>et al</i> 2010)
Φ_f	0.16 ^c	0.05 (Aveline <i>et al</i> 1994)	0.14 (Milanesio <i>et al</i> 2001)	0.16 (Redmond and Gamlin 1999)
τ_T (s)	$(6.3 \pm 1.2) \times 10^{-9}$ (Russell <i>et al</i> 2008)	5.2×10^{-9} (Aveline <i>et al</i> 1994)	7.5×10^{-9} (Kress <i>et al</i> 2003)	$(5.5 \pm 1.2) \times 10^{-9}$ (Russell <i>et al</i> 2008)

(Continued)

Table 5. (Continued)

Parameter	HPPH	LS11	mLu	Pc 4	WST09	WST11
(b) Non-FDA or EMA approved common photosensitizers						
ϵ ($\mu\text{M}^{-1} \text{cm}^{-1}$)	0.109 @665 nm (Bellnier <i>et al</i> 2003)	0.040 @654 nm (Spikes and Bommer 1993b)	0.0312 @732 nm (Zhu <i>et al</i> 2003)	0.200 @675 nm (Baron <i>et al</i> 2010)	0.09296 @762 nm (Weersink <i>et al</i> 2005b)	0.12 @ 752 nm (Price <i>et al</i> 2013)
k_0 @ 100 mW cm^{-2} (s^{-1})	60.55 ^a	21.85 ^a	19.08 ^a	112.78 ^a	59.17 ^a	75.39 ^a
k_1 ($\mu\text{M}^{-1} \text{s}^{-1}$)	1×10^{2b}	1.14×10^{4l} (Spikes and Bommer 1993a)	$(\sim 1 \times 10^2)^m$	—	$(1.6 \times 10^2)^n$	1.6×10^{2b}
k_2 ($\mu\text{M}^{-1} \text{s}^{-1}$)	3×10^3 $(2.5\text{--}3.4) \times 10^3$ (Pandey <i>et al</i> 1996)	1.9×10^3 $(1.3\text{--}1.9) \times 10^3$ (Spikes and Bommer 1993b)	1.3×10^3 (Guldi <i>et al</i> 2000)	3.83×10^3 (He <i>et al</i> 1997)	2.2×10^3 (Vakrat-Hagili <i>et al</i> 2005)	$(\sim 2.2 \times 10^3)^p$
k_3 (s^{-1})	$(8 \times 10^6)^d$	6.0×10^{7d}	1.58×10^{9d}	$(1 \times 10^8)^d$	1.7×10^{10} (Vakrat-Hagili <i>et al</i> 2005)	$(1.7 \times 10^{10})^p$
k_4 (s^{-1})	3.6×10^{4e}	1.4×10^4 $(1.4\text{--}1.9) \times 10^4$ (Ohmori <i>et al</i> 2007)	1.5×10^{4e}	4.6×10^{4e}	2.6×10^{4e}	$(\sim 2.6 \times 10^4)^p$
k_5 (s^{-1})	$(1.92 \times 10^8)^f$	2.4×10^{8f}	8.31×10^{8f}	$(1 \times 10^8)^f$	8.33×10^{11f}	$(\sim 8.33 \times 10^{11})^p$
k_6 (s^{-1})	3.3×10^{5g}	3.3×10^{5g}	3.3×10^{5g}	3.3×10^{5g}	3.3×10^{5g}	3.3×10^{5g}
$k_7[A]$ (s^{-1})	1×10^{7h} $(3 \times 10^6\text{--}3 \times 10^7)$ $(0)^j$	1×10^{7h} $(3 \times 10^6\text{--}3 \times 10^7)$ $(0)^j$	1×10^{7h} $(3 \times 10^6\text{--}3 \times 10^7)$ $(0)^j$	1×10^{7h} $(3 \times 10^6\text{--}3 \times 10^7)$ $(0)^j$	$(1 \times 10^7)^q$ $(3 \times 10^6\text{--}3 \times 10^7)$ $(0)^j$	$(1 \times 10^7)^q$ $(3 \times 10^6\text{--}3 \times 10^7)$ $(0)^j$
$k_8[A]$ (s^{-1})	$(11.9)^c$	7.4 ^r	$(11.9)^c$	$(11.9)^c$	$(11.9)^c$	$(11.9)^c$
β (μM)	$(33)^c$	$(33)^c$	$(33)^c$	$(33)^c$	$(33)^c$	$(33)^c$
δ (μM)	$(70 \pm 40) \times 10^{-3}$ (Penjweini <i>et al</i> 2015b)	$(36.8 \times 10^{-3})^s$	$(13.8 \times 10^{-3})^s$	$(118.7 \times 10^{-3})^s$	122×10^{-3t}	$(155.5 \times 10^{-3})^t$
ξ ($\text{cm}^2 \text{mW}^{-1} \text{s}^{-1}$)	$1 \pm 6 \times 10^{-5}$ (Penjweini <i>et al</i> 2015b)	1.14×10^{-3u}	1×10^{-5u}	—	1.6×10^{-5u}	$(1.6 \times 10^{-5})^p$
σ (μM^{-1})	$(0)^i$	$(0)^i$	$(0)^i$	$(0)^i$	—	—
η ($\text{cm}^2 \text{mW}^{-1} \text{s}^{-1} \mu\text{M}$)	$(0)^i$	$(0)^i$	$(0)^i$	$(0)^i$	—	—

(Continued)

Table 5. (Continued)

Parameter	HPPH	LS11	mLu	Pc 4	WST09	WST11
g ($\mu\text{M s}^{-1}$)	1.5 ± 0.9 (Penjweini <i>et al</i> 2015b)	—	—	—	—	—
S_{Δ} or S_I	0.12^y	$(0.211)^y$	$(0.211)^y$	$(0.211)^y$	0.211^v	$(0.211)^p$
Φ_t	0.96 0.48 – 1 (Bellnier <i>et al</i> 2003)	$0.8 > 0.8$ (Ohmori and Arai 2006)	0.344 (Guldi <i>et al</i> 2000)	$(-0.5)^w$	0.98 (Weersink <i>et al</i> 2005b)	$(0.98)^p$
Φ_{Δ} or Φ_{ROS}	0.12^x (0.48) (Bellnier <i>et al</i> 2003)	0.17^x (0.77) (Spikes and Bommer 1993b) $(0.61$ – $0.77)$	0.073^x (0.31) (Guldi <i>et al</i> 2000)	0.11^x (0.43) (He <i>et al</i> 1997)	0.21^x $(0.1$ – $1)$ (Vakrat-Haglili <i>et al</i> 2005, Ormond and Freeman 2013)	$(0.21)^p$
Φ_T	0.43 (Pandey <i>et al</i> 1996)	0.008 – 0.010 (Li <i>et al</i> 2002)	0.01 – 0.015 (Guldi <i>et al</i> 2000, Lovell <i>et al</i> 2010)	0.62 – 0.8 (Nyokong 2007)	$< 0.01^y$	$< 0.01^y$
τ_T (s)	$(-5 \times 10^{-9})^z$	$(3.3$ – $3.8) \times 10^{-9}$ (Li <i>et al</i> 2002)	4.14×10^{-10} (Guldi <i>et al</i> 2000)	$(4.59 \pm 0.03) \times 10^{-9}$ (Zhao <i>et al</i> 2009)	$1.2 \times 10^{-12\text{aa}}$	$(1.2 \times 10^{-12})^p$

^a Calculated based on value of ε and $\phi = 100 \text{ mW cm}^{-2}$; $k_0 = \varepsilon\phi(h\nu)$, ALA-PPHX: $k_0 = (0.003 \mu\text{M}^{-1} \text{cm}^{-1}) / (6.022 \times 10^{14} \text{ cm}^2 \mu\text{M}^{-1}) \times (100 \text{ mW cm}^{-2}) / (3.14 \times 10^{-16} \text{ mW s}) = 1.59 \text{ s}^{-1}$, BPD: $k_0 = (0.0783 \mu\text{M}^{-1} \text{cm}^{-1}) / (6.022 \times 10^{14} \text{ cm}^2 \mu\text{M}^{-1}) \times (100 \text{ mW cm}^{-2}) / (2.88 \times 10^{-16} \text{ mW s}) = 45.13 \text{ s}^{-1}$, mTHPC: $k_0 = (0.111 \mu\text{M}^{-1} \text{cm}^{-1}) / (6.022 \times 10^{14} \text{ cm}^2 \mu\text{M}^{-1}) \times (100 \text{ mW cm}^{-2}) / (3.06 \times 10^{-16} \text{ mW s}) = 60.27 \text{ s}^{-1}$, Photofrin: $k_0 = (0.0035 \mu\text{M}^{-1} \text{cm}^{-1}) / (6.022 \times 10^{14} \text{ cm}^2 \mu\text{M}^{-1}) \times (100 \text{ mW cm}^{-2}) / (3.16 \times 10^{-16} \text{ mW s}) = 1.84 \text{ s}^{-1}$, HPPH: $k_0 = (0.109 \mu\text{M}^{-1} \text{cm}^{-1}) / (6.022 \times 10^{14} \text{ cm}^3 \mu\text{M}^{-1}) \times (100 \text{ mW cm}^{-2}) / (2.99 \times 10^{-16} \text{ mW s}) = 60.55 \text{ s}^{-1}$, LS11: $k_0 = (0.040 \mu\text{M}^{-1} \text{cm}^{-1}) / (6.022 \times 10^{14} \text{ cm}^3 \mu\text{M}^{-1}) \times (100 \text{ mW cm}^{-2}) / (3.04 \times 10^{-16} \text{ mW s}) = 21.85 \text{ s}^{-1}$, mLu: $k_0 = (0.0312 \mu\text{M}^{-1} \text{cm}^{-1}) / (6.022 \times 10^{14} \text{ cm}^3 \mu\text{M}^{-1}) \times (100 \text{ mW cm}^{-2}) / (2.72 \times 10^{-16} \text{ mW s}) = 19.08 \text{ s}^{-1}$, Pc 4: $k_0 = (0.200 \mu\text{M}^{-1} \text{cm}^{-1}) / (6.022 \times 10^{14} \text{ cm}^3 \mu\text{M}^{-1}) \times (100 \text{ mW cm}^{-2}) / (2.94 \times 10^{-16} \text{ mW s}) = 112.78 \text{ s}^{-1}$, WST09: $k_0 = (0.09296 \mu\text{M}^{-1} \text{cm}^{-1}) / (6.022 \times 10^{14} \text{ cm}^3 \mu\text{M}^{-1}) \times (100 \text{ mW cm}^{-2}) / (2.61 \times 10^{-16} \text{ mW s}) = 59.17 \text{ s}^{-1}$, WST11: $k_0 = (0.12 \mu\text{M}^{-1} \text{cm}^{-1}) / (6.022 \times 10^{14} \text{ cm}^3 \mu\text{M}^{-1}) \times (100 \text{ mW cm}^{-2}) / (2.64 \times 10^{-16} \text{ mW s}) = 75.39 \text{ s}^{-1}$.
^b Calculated based on value of σ and k_2 ; $k_1 = \sigma \times k_2[A]$, ALA-PPHX: $k_1 = (9 \times 10^{-5} \mu\text{M}^{-1}) \times (1 \times 10^7 \text{ s}^{-1}) = 9 \times 10^2 \mu\text{M}^{-1} \text{ s}^{-1}$, BPD: $k_1 = (1.7 \times 10^{-5} \mu\text{M}^{-1}) \times (1 \times 10^7 \text{ s}^{-1}) = 1.7 \times 10^2 \mu\text{M}^{-1} \text{ s}^{-1}$, mTHPC: $k_1 = (2.97 \times 10^{-5} \mu\text{M}^{-1}) \times (1 \times 10^7 \text{ s}^{-1}) = 2.97 \times 10^2 \mu\text{M}^{-1} \text{ s}^{-1}$, Photofrin: $k_1 = (7.6 \times 10^{-5} \mu\text{M}^{-1}) \times (1 \times 10^7 \text{ s}^{-1}) = 7.6 \times 10^2 \mu\text{M}^{-1} \text{ s}^{-1}$, HPPH: $k_1 = (1 \times 10^{-5} \mu\text{M}^{-1}) \times (1 \times 10^7 \text{ s}^{-1}) = 1 \times 10^2 \mu\text{M}^{-1} \text{ s}^{-1}$, $k_1 = k_{11}$ and $k_1 = k_{12}$ for type II PS and $k_1 = k_{11}$ for type I PS.
^c Assumed to be similar to the values for Photofrin.

(Continued)

^d Calculated based on the value of ϕ_1 and τ_1 : $k_3 = (1 - \phi_1)/\tau_1$. BPD: $k_3 = (1 - 0.79)/(5.2 \times 10^{-9} \text{ s}) = 4.04 \times 10^7 \text{ s}^{-1}$. mTHPC: $k_3 = (1 - 0.89)/(7.5 \times 10^{-9} \text{ s}) = 1.47 \times 10^7 \text{ s}^{-1}$. HPPH: $k_3 = (1 - 0.96)/(5 \times 10^{-9} \text{ s}) = 8 \times 10^6 \text{ s}^{-1}$. LS11: $k_3 = (1 - 0.8)/(3.3 \times 10^{-9} \text{ s}) = 6 \times 10^7 \text{ s}^{-1}$. Mlu: $k_3 = (1 - 0.344)/(4.14 \times 10^{-10} \text{ s}) = 1.58 \times 10^9 \text{ s}^{-1}$. PC4: $k_3 = (1 - 0.5)/(4.6 \times 10^{-9} \text{ s}) = 1 \times 10^8 \text{ s}^{-1}$.

^e Calculated based on value of β and k_2 : $k_4 = \beta \times k_2$. ALA-PPIX: $k_4 = (11.9 \mu\text{M}) \times (1.9 \times 10^3 \mu\text{M}^{-1} \text{ s}^{-1}) = 2.3 \times 10^4 \text{ s}^{-1}$. BPD: $k_4 = (11.9 \mu\text{M}) \times (3 \times 10^3 \mu\text{M}^{-1} \text{ s}^{-1}) = 3.6 \times 10^4 \text{ s}^{-1}$. mTHPC: $k_4 = (8.7 \mu\text{M}) \times (2.6 \times 10^3 \mu\text{M}^{-1} \text{ s}^{-1}) = 2.3 \times 10^4 \text{ s}^{-1}$. Photofrin: $k_4 = (11.9 \mu\text{M}) \times (1.4 \times 10^3 \mu\text{M}^{-1} \text{ s}^{-1}) = 1.67 \times 10^4 \text{ s}^{-1}$. HPPH: $k_4 = (11.9 \mu\text{M}) \times (3 \times 10^3 \mu\text{M}^{-1} \text{ s}^{-1}) = 3.6 \times 10^4 \text{ s}^{-1}$. mLu: $k_4 = (11.9 \mu\text{M}) \times (1.3 \times 10^3 \mu\text{M}^{-1} \text{ s}^{-1}) = 1.4 \times 10^4 \text{ s}^{-1}$. Pc4: $k_4 = (11.9 \mu\text{M}) \times (3.83 \times 10^3 \mu\text{M}^{-1} \text{ s}^{-1}) = 4.6 \times 10^4 \text{ s}^{-1}$. WST09: $k_4 = (11.9 \mu\text{M}) \times (2.2 \times 10^3 \mu\text{M}^{-1} \text{ s}^{-1}) = 2.6 \times 10^4 \text{ s}^{-1}$.

^f Calculated based on value of k_3 and ϕ_2 : $k_5 = \phi_2 k_3 / (1 - \phi_2)$. ALA-PPIX: $k_5 = (0.83) \times 2.9 \times 10^7 \text{ s}^{-1} / (1 - 0.83) = 1.2 \times 10^7 \text{ s}^{-1}$. BPD: $k_5 = (0.79) \times 4.04 \times 10^7 \text{ s}^{-1} / (1 - 0.79) = 1.52 \times 10^7 \text{ s}^{-1}$. mTHPC: $k_5 = (0.89) \times 1.47 \times 10^7 \text{ s}^{-1} / (1 - 0.89) = 1.19 \times 10^7 \text{ s}^{-1}$. Photofrin: $k_5 = (0.63) \times 2.9 \times 10^7 \text{ s}^{-1} / (1 - 0.63) = 4.94 \times 10^7 \text{ s}^{-1}$. HPPH: $k_5 = (0.96) \times (8 \times 10^6 \text{ s}^{-1}) / (1 - 0.96) = 1.92 \times 10^8 \text{ s}^{-1}$. LS11: $k_5 = (0.8) \times (6 \times 10^7 \text{ s}^{-1}) / (1 - 0.8) = 2.4 \times 10^8 \text{ s}^{-1}$. mLu: $k_5 = (0.344) \times (1.58 \times 10^9 \text{ s}^{-1}) / (1 - 0.344) = 8.31 \times 10^8 \text{ s}^{-1}$. Pc4: $k_5 = (0.5) \times (1 \times 10^8 \text{ s}^{-1}) / (1 - 0.5) = 1 \times 10^8 \text{ s}^{-1}$. WST09: $k_5 = (0.98) \times (1.7 \times 10^{10} \text{ s}^{-1}) / (1 - 0.98) = 8.33 \times 10^{11} \text{ s}^{-1}$.

^g $\tau_{\Delta} = 3 \mu\text{s}$ in water and $0.16 \mu\text{s}$ in tissue (Dysart *et al* 2005). $k_6 = \tau_{\Delta}^{-1} - k_7[A] = (3 \mu\text{s})^{-1} = 3.3 \times 10^5 \text{ s}^{-1}$.

^h $k_7[A] = \tau_{\Delta}^{-1} - k_6 = (0.1 \mu\text{s})^{-1} - (3.3 \times 10^5 \text{ s}^{-1}) = 1 \times 10^7 \text{ s}^{-1}$, taken from Zhu *et al* (2015b). The value of $[A]$ is unknown but can be estimated from the value of $k_7 = 235 \mu\text{M}^{-1} \text{ s}^{-1}$. For a well-known singlet oxygen quencher, $\text{Na}_2\text{S}_2\text{O}_3$ (Kim *et al* 2016): $[A] = 10^7 \text{ s}^{-1} / 235 \mu\text{M}^{-1} \text{ s}^{-1} = 42 \text{ mM}$. The magnitude of $[A]$ is reasonable considering the singlet oxygen threshold dose can be up to 12 mM (Zhu *et al.*, 2014), without causing any effect on singlet oxygen lifetime. $k_7 = k_{71} + k_{72}$. k_7 is assumed to be $k_7 = k_{72}$ for type II PS and $k_7 = k_{71}$ for type I PS.

ⁱ Assume no hypoxic interaction.

^j *In vivo* values calculated based on the values of ξ , ϕ_1 , and ε : $S_{\Delta} = \xi \phi_1 \varepsilon \times (hv)$. ALA-PPIX: $S_{\Delta} = (3.7 \times 10^{-3} \text{ cm}^2 \text{ mW}^{-1} \text{ s}^{-1}) / (0.83) / (0.003 \mu\text{M}^{-1} \text{ cm}^{-1}) \times (6.022 \times 10^{14} \text{ cm}^3 \mu\text{M}^{-1}) \times (3.14 \times 10^{-16} \text{ mW s}) = 0.281$. BPD: $S_{\Delta} = (51 \times 10^{-3} \text{ cm}^2 \text{ mW}^{-1} \text{ s}^{-1}) / (0.79) / (0.0312 \mu\text{M}^{-1} \text{ cm}^{-1}) \times (6.022 \times 10^{14} \text{ cm}^3 \mu\text{M}^{-1}) \times (2.72 \times 10^{-16} \text{ mW s}) = 0.144$. mTHPC: $S_{\Delta} = (30 \times 10^{-3} \text{ cm}^2 \text{ mW}^{-1} \text{ s}^{-1}) / (0.89) / (0.111 \mu\text{M}^{-1} \text{ cm}^{-1}) \times (6.022 \times 10^{14} \text{ cm}^3 \mu\text{M}^{-1}) \times (3.06 \times 10^{-16} \text{ mW s}) = 0.056$. Photofrin: $S_{\Delta} = (3.7 \times 10^{-3} \text{ cm}^2 \text{ mW}^{-1} \text{ s}^{-1}) / (0.63) / (0.0035 \mu\text{M}^{-1} \text{ cm}^{-1}) \times (6.022 \times 10^{14} \text{ cm}^3 \mu\text{M}^{-1}) \times (3.16 \times 10^{-16} \text{ mW s}) = 0.319$.

^k *In vivo* values calculated based on the values of S_{Δ} and ϕ_1 : $\phi_{\Delta} = S_{\Delta} \times \phi_1$. ALA-PPIX: $\phi_{\Delta} = (0.281) \times (0.83) = 0.233$. BPD: $\phi_{\Delta} = (0.144) \times (0.83) = 0.114$. mTHPC: $\phi_{\Delta} = (0.104) \times (0.89) = 0.093$. Photofrin: $\phi_{\Delta} = (0.319) \times (0.63) = 0.20$.

^l Calculated based on quantum yield of photobleaching being 15 times larger than that of Photofrin (Spikes and Bommer 1993a).

^m Assumed value to be in the same order of magnitude as that of HPPH due to the low photobleaching characteristics.

ⁿ Assumed to be the same as that of WST11.

^o Calculated based on analysis of photobleaching data from (Price *et al* 2013).

^p Assumed to be the same as that of WST09 and all photosensitizers having values of the same order of magnitude.

^q Assume tissue damage due to type I action is the same as that due to type II action, i.e. $k_{71}[A] = k_{72}[A]$.

^r Calculated based on value of k_2 and k_4 : $\beta = k_4/k_2 = (1.4 \times 10^4 \text{ s}^{-1}) / (1.9 \times 10^3 \mu\text{M}^{-1} \text{ s}^{-1}) = 7.4 \mu\text{M}$.

(Continued)

^s Calculated based on value of ξ for Photofrin: $\xi = \xi_{\text{phot}} \times (\varepsilon/\varepsilon_{\text{phot}}) \times (h\nu_{\text{phot}}/h\nu) \times (\Phi_f/\Phi_{\text{L,phot}}) \times (\Phi_f/\Phi_{\text{L,phot}}) \times (0.66)$ where 0.66 is the average value of $\xi_{\text{experimental}}/\xi_{\text{calculated}}$ for Photofrin, ALA, BPD, mTHPC, and HPPH. LS11: $\xi = (3.7 \times 10^{-3} \text{ cm}^2 \text{ mW}^{-1} \text{ s}^{-1}) \times (0.04 \mu\text{M}^{-1} \text{ cm}^{-1} \text{ mW}^{-1} \text{ cm}^{-1}) \times (3.16 \times 10^{-16} \text{ mW s}/3.04 \times 10^{-16} \text{ mW s}) \times (0.8/0.63) \times 0.66 = 36.8 \times 10^{-3} \text{ cm}^2 \text{ mW}^{-1} \text{ s}^{-1}$, mLu: $\xi = (3.7 \times 10^{-3} \text{ cm}^2 \text{ mW}^{-1} \text{ s}^{-1}) \times (0.0312 \mu\text{M}^{-1} \text{ cm}^{-1} \text{ mW}^{-1} \text{ cm}^{-1}) \times (3.16 \times 10^{-16} \text{ mW s}/2.72 \times 10^{-16} \text{ mW s}) \times (0.344/0.63) \times 0.66 = 13.8 \times 10^{-3} \text{ cm}^2 \text{ mW}^{-1} \text{ s}^{-1}$, Pc 4: $\xi = (3.7 \times 10^{-3} \text{ cm}^2 \text{ mW}^{-1} \text{ s}^{-1}) \times (0.200 \mu\text{M}^{-1} \text{ cm}^{-1} \text{ mW}^{-1} \text{ cm}^{-1}) \times (3.16 \times 10^{-16} \text{ mW s}/2.94 \times 10^{-16} \text{ mW s}) \times (0.5/0.63) \times 0.66 = 118.7 \times 10^{-3} \text{ cm}^2 \text{ mW}^{-1} \text{ s}^{-1}$, where the value of Φ_f was assumed to be 0.5.

^t Calculated based on value of ξ for Photofrin: $\xi = \xi_{\text{phot}} \times (\varepsilon/\varepsilon_{\text{phot}}) \times (h\nu_{\text{phot}}/h\nu) \times (\Phi_f/\Phi_{\text{L,phot}}) \times (\Phi_f/\Phi_{\text{L,phot}}) \times (0.66)$ where 0.66 is the average value of $\xi_{\text{experimental}}/\xi_{\text{calculated}}$ for Photofrin, ALA, BPD, mTHPC, and HPPH. Notice that ξ here is due to type I interaction, S_I , rather than type II interaction, S_{II} . We have assumed $S_I/S_{II} = 0.66$ between WST09 (or WST11) and Photofrin.

WST09: $\xi = (3.7 \times 10^{-3} \text{ cm}^2 \text{ mW}^{-1} \text{ s}^{-1}) \times (0.09296 \mu\text{M}^{-1} \text{ cm}^{-1} \text{ mW}^{-1} \text{ cm}^{-1}) \times (3.16 \times 10^{-16} \text{ mW s}/2.61 \times 10^{-16} \text{ mW s}) \times (0.98/0.63) \times 0.66 = 122 \times 10^{-3} \text{ cm}^2 \text{ mW}^{-1} \text{ s}^{-1}$.

WST11: $\xi = (3.7 \times 10^{-3} \text{ cm}^2 \text{ mW}^{-1} \text{ s}^{-1}) \times (0.12 \mu\text{M}^{-1} \text{ cm}^{-1} \text{ mW}^{-1} \text{ cm}^{-1}) \times (3.16 \times 10^{-16} \text{ mW s}/2.64 \times 10^{-16} \text{ mW s}) \times (0.98/0.63) \times 0.66 = 155.5 \times 10^{-3} \text{ cm}^2 \text{ mW}^{-1} \text{ s}^{-1}$.

^u Calculated based on value of k_1 and $k_7[A]$: LS11: $\sigma = k_1/k_7[A]$; LS11: $\sigma = (1.4 \times 10^5 \mu\text{M}^{-1} \text{ s}^{-1})/(1 \times 10^7 \text{ s}^{-1}) = 1.4 \times 10^{-3} \mu\text{M}^{-1}$, WST09: $\sigma = (1.6 \times 10^2 \mu\text{M}^{-1} \text{ s}^{-1})/(1 \times 10^7 \text{ s}^{-1}) = 1.6 \times 10^{-5} \mu\text{M}^{-1}$, MLu: $\sigma = (1 \times 10^2 \mu\text{M}^{-1} \text{ s}^{-1})/(1 \times 10^7 \text{ s}^{-1}) = 1 \times 10^{-5} \mu\text{M}^{-1}$, $\sigma = (\xi_{\text{total}} + \xi_{\text{int}})/\xi$ and it is assumed $\sigma_I \sim 0$ for type II PS and $\sigma_{II} \sim 0$ for type I PS.

^v Calculated based on the values of ξ , Φ_f , and ε : $S_{II} = \xi\Phi_f/\varepsilon \times (h\nu)$ for type II or $S_I = \xi\Phi_f/\varepsilon \times (h\nu)$ for type I. LS11: $S_{II} = (36.8 \times 10^{-3} \text{ cm}^2 \text{ mW}^{-1} \text{ s}^{-1})/(0.8)$ (0.04 $\mu\text{M}^{-1} \text{ cm}^{-1}$) $\times (6.022 \times 10^{14} \text{ cm}^2 \mu\text{M}^{-1}) \times (3.04 \times 10^{-16} \text{ mW s}) = 0.211$, mLu: $S_{II} = (13.8 \times 10^{-3} \text{ cm}^2 \text{ mW}^{-1} \text{ s}^{-1})/(0.344)/(0.0312 \mu\text{M}^{-1} \text{ cm}^{-1}) \times (6.022 \times 10^{14} \text{ cm}^2 \mu\text{M}^{-1}) \times (2.72 \times 10^{-16} \text{ mW s}) = 0.211$, WST09: $S_I = (122 \times 10^{-3} \text{ cm}^2 \text{ mW}^{-1} \text{ s}^{-1})/(0.98)/(0.09296 \mu\text{M}^{-1} \text{ cm}^{-1}) \times (6.022 \times 10^{14} \text{ cm}^2 \mu\text{M}^{-1}) \times (2.61 \times 10^{-16} \text{ mW s}) = 0.211$

^w Assumed value of Φ_f that is of the same order of magnitude as that of other photosensitizers to be used in calculations.

^x *In vivo* values calculated based on the values of S_{II} (or S_I) and Φ_f : $\Phi_{\Delta} = S_{II} \times \Phi_f$ for type II or $\Phi_{\text{ROS}} = S_I \times \Phi_f$ for type I. HPPH: $\Phi_{\Delta} = (0.12) \times (0.96) = 0.12$, LS11: $\Phi_{\Delta} = (0.211) \times (0.8) = 0.17$, mLu: $\Phi_{\Delta} = (0.211) \times (0.344) = 0.073$, Pc 4: $\Phi_{\Delta} = (0.211) \times (0.5) = 0.11$, WST09: $\Phi_{\text{ROS}} = (0.211) \times (0.98) = 0.21$.

^y Assumed to be <0.01 due to the lack of fluorescence signal for WST09 and WST11 (Vakrat-Hagjili *et al* 2005).

^z Assumed value to be in the same order of magnitude as other type II photosensitizers.

^{aa} Calculated based on value of k_3 and k_5 : $\tau_I = 1/(k_3 + k_5)$, WST-09: $\tau_I = 1/(1.7 + 83.3) \times 10^{10} \text{ s}^{-1} = 1.2 \times 10^{-12} \text{ s}$.

Note. Each parameter is given a default value first, which is the *in vivo* value consistent between parameters used in the table. A range for each parameter is provided next, mostly based on *in vitro* measurement from literature. References, whenever existed, are provided for each parameter. When a parameter does not exist in the literature but can be estimated based on our review, it is presented in parenthesis. We use a ‘—’ to represent parameters that are unknown at the time of the review.

6. Conclusions

During PDT, energy from the triplet-state photosensitizer excited via the absorption of light is transferred to ground-state oxygen, which produces ROS. Mathematical models have been developed to simulate the process of PDT for both type I and II PS. These models use a set of differential equations describing the major photochemical reaction pathways in PDT to calculate temporal and spatial distributions of singlet oxygen, ground-state oxygen, and the photosensitizer.

This review summarizes known photochemical parameters, methods to determine the rate constants, and other key photochemical parameters (some of which are *in vivo*). It is found that many fundamental rate constant values are unavailable for many common PS, and experimental efforts to determine these parameters are required in order to perform explicit dosimetry of ROS.

There is great potential for future work to determine *in vivo* photochemical rate parameters for use in PDT modeling and dosimetry. However, further studies are needed to determine these parameters *in vivo*. For a particular photosensitizer to be studied in pre-clinical and clinical dosimetry studies, it is important to have the complete set of photophysical and photochemical parameters.

Acknowledgments

For TCZ and MMK, this work is supported by grants from National Institute of Health (NIH) R01 CA154562 and P01 CA87971. AAG and AG acknowledge support the National Science Foundation, Division of Chemistry: CHE1464975 and PSC-CUNY (68125-0046). We thank Leda Lee for the graphic arts work.

Appendix A. Biological and other examples of singlet oxygen reactions

Biological compounds such as imidazole and guanine can react with $^1\text{O}_2$ by [2 + 4] cycloaddition to form endoperoxide, which can be characterized at low temperature (figure A1) (Sheu and Foote 1993). DNA base pairs can also undergo tandem reactions with $^1\text{O}_2$ to form spirodiimidohydantoin species (figure A2) (Hickerson *et al* 1999, McCallum *et al* 2004, Di Mascio *et al* 2014). Conjugated dienes can also undergo tandem reactions with $^1\text{O}_2$ to form allylic hydroperoxides followed by 1,4-endoperoxides (figure A3). These kinds of conjugated alkenes are common in natural products and lipids in biological systems (Blay *et al* 2005).

Singlet oxygen reacts with electron-rich alkene by [2 + 2] cycloadditions to give mono and bis bicyclic dioxetanes that can chemiluminesce upon decomposition (figure A4) (Zaklika *et al* 1978, Adam *et al* 1979). The decomposition of endoperoxide can provide for a chemical source of $^1\text{O}_2$, e.g., naphthalene and anthracene (figure A5) (Wasserman and Larsen 1972, Fudickar and Linker 2014, Klaper and Linker 2015). Photosensitizers such as dyes, pharmaceuticals, and cosmetics can serve as photodynamic agents and produce $^1\text{O}_2$. A variety of chromophore-rich natural products can sensitize organisms to damage by singlet oxygenation, including chlorophyll, metal-less porphyrins, flavins, polyacetylenes, pigments, and mold toxins (Wasserman and Murray 1979).

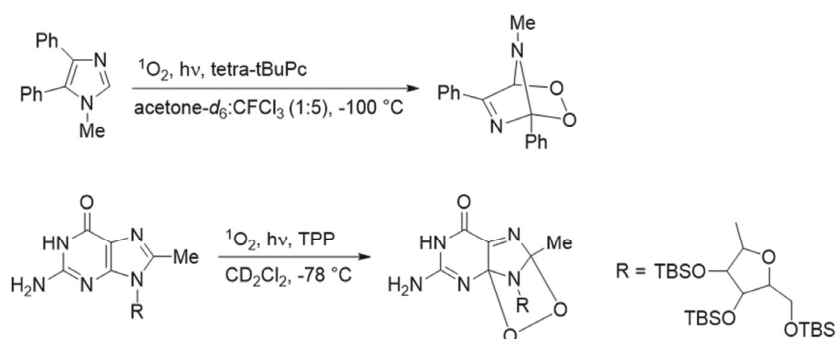


Figure A1. Reaction of imidazole (top) and guanine (bottom) with $^1\text{O}_2$ to form endoperoxides. tetra-*t*BuPc = tetra-*t*-butylphthalocyanines and TPP = tetraphenylporphyrin photosensitizers, CD_2Cl_2 = chloroform- d_2 and CFCl_3 = trichlorofluoromethane solvent.

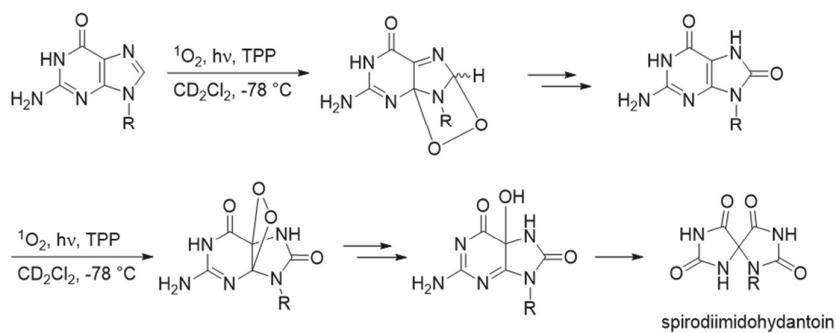


Figure A2. Reaction of DNA basepairs with $^1\text{O}_2$ to form spirodiimidohydantoin. TPP = tetraphenylporphyrin photosensitizer and CD_2Cl_2 = chloroform- d_2 solvent.

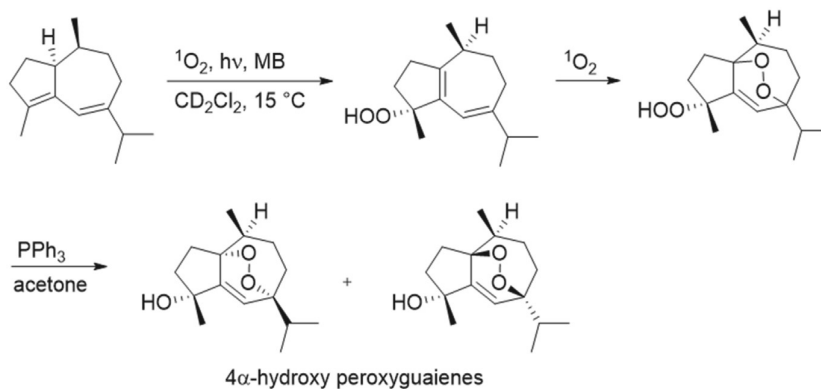


Figure A3. Reaction of conjugated dienes with $^1\text{O}_2$ to form allylic hydroperoxides, followed by 1,4-endoperoxides. MB = methylene blue photosensitizer, CD_2Cl_2 = chloroform- d_2 solvent and PPh_3 = triphenylphosphine.

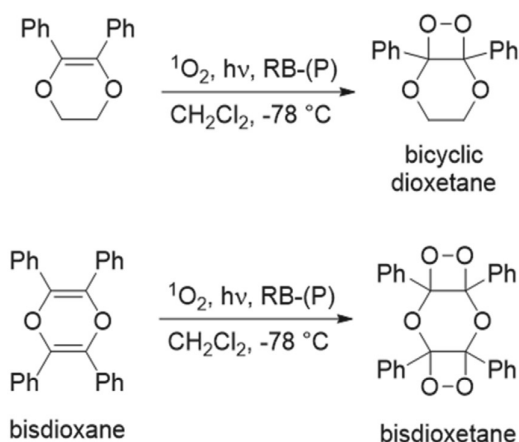


Figure A4. Top: reaction of alkene with $^1\text{O}_2$ to form bicyclic dioxetanes. Bottom: Reaction of bisdioxane with $^1\text{O}_2$ to form bisdioxetane. RB-(P) = rose bengal photosensitizer immobilized on polymer support and CH_2Cl_2 = dichloromethane solvent.

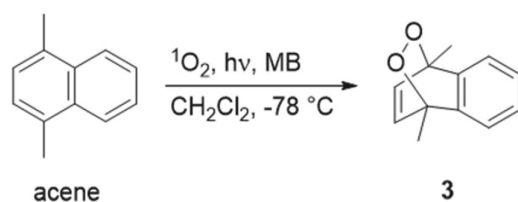


Figure A5. Reaction of acene with $^1\text{O}_2$ to form endoperoxide. MB = methylene blue photosensitizer and CH_2Cl_2 = dichloromethane solvent.

Appendix B. Microscopic singlet oxygen model

With the microscopic singlet oxygen model, the tumor is assumed to have uniformly distributed capillaries aligned parallel to the linear light source. The inter-capillary distance between two adjacent capillaries is large enough so that each one can supply oxygen only to its immediate, concentric surrounding tissue. A Krogh cylinder model can be adapted for a single capillary and its surrounding tissue. The 3D Krogh model can be simplified into a 2D, cylindrically symmetric model. Under normal situations, the red blood cell (RBC) contains hemoglobin, which is where hemoglobin saturation and desaturation occurs. After oxygen unloads from oxy-hemoglobin, it will diffuse into the blood through the RBC membrane and into the tissue. The microscopic model assumes that there is no oxygen diffusion barrier in the RBC membrane, and that the distribution of hemoglobin within the capillary is uniform. Given these assumptions, the time-dependent governing equations for $^3\text{O}_2$ and hemoglobin transport inside the capillary are given by (Zhu *et al* 2015c)

$$\alpha_c \frac{\partial P}{\partial t} = \alpha_c D_c \nabla^2 P - v \cdot \alpha_c \nabla P + \Gamma_{\text{ox}}, \quad (\text{B.1})$$

$$C_H \frac{\partial Sa}{\partial t} = C_H D_H \nabla^2 Sa - v \cdot C_H \nabla Sa - \Gamma_{\text{ox}}, \quad (\text{B.2})$$

where Sa denotes the hemoglobin oxygen saturation describing the percentage of hemoglobin oxygen concentration to the total hemoglobin concentration, Γ_{ox} is the 'reaction' term representing the $^3\text{O}_2$ loading/unloading from deoxyhemoglobin/oxyhemoglobin. D_c and D_h represent the diffusion coefficients of $^3\text{O}_2$ and hemoglobin in the capillary respectively. α_c is the solubility of $^3\text{O}_2$ in plasma and v is the blood velocity in the capillary. The concentration of $^3\text{O}_2$ is expressed using the partial pressure (P) of $^3\text{O}_2$ and the oxygen solubility coefficient (a) based on

$$[^3\text{O}_2] = \alpha P. \quad (\text{B.3})$$

Oxygen concentration can be expressed using oxygen partial pressure. The oxygen supply term (Γ) for equation (18) is given by

$$\Gamma = D_t \nabla^2 [^3\text{O}_2] - q_0 \frac{[^3\text{O}_2]}{[^3\text{O}_2] + \alpha_t P_m}, \quad (\text{B.4})$$

where q_0 is the maximum metabolic oxygen consumption rate in the Michaelis–Menten relationship (Hudson and Cater 1964) for the microscopic model, D_t is the $^3\text{O}_2$ diffusion coefficient in tissue, and P_m is the $^3\text{O}_2$ partial pressure at half maximum $^3\text{O}_2$ consumption concentration. As well as in a vascular medium

$$\Gamma = D_s \nabla^2 [^3\text{O}_2], \quad (\text{B.5})$$

where D_s is the $^3\text{O}_2$ diffusion coefficient in vascular media.

Unless the microscopic vascular structures are known or important for the purpose of the model, it is often unnecessary to model the oxygen diffusion process if the vessels are assumed to be uniformly distributed because the oxygen diffusion typically happens at a spatial scale of less than 50 μm and the details of oxygen diffusion have little impact on light transport or drug distribution, which often happen in the mm spatial scale. Microscopic modeling should explain subtle details of tissue reoxygenation after interruptions of the light irradiation at appropriate intervals (fractionated PDT), which may not be completely modeled in a macroscopic model.

References

- Adam W 1981 The singlet oxygen story *Chem. unserer Zeit* **15** 190–6
- Adam W, Cheng C C, Cueto O, Erden I and Zinner K 1979 A stable bisdioxetane *J. Am. Chem. Soc.* **101** 4735–6
- Adam W and Trofimov A V 2006 *Chemistry of Peroxides* vol 2, ed Z Rappoport (Chichester: John Wiley & Sons Ltd) pp 1171–209
- Agostinis P *et al* 2011 Photodynamic therapy of cancer: an update *CA Cancer J. Clin.* **61** 250–81
- Arnfield M R, Chapman J D, Tulip J, Fenning M C and PMcPhee M S 1993 Optical properties of experimental prostate tumors *in vivo Photochem. Photobiol.* **57** 306–11
- Arnold S J, Ogryzlo E A and Witzke H 1964 Some new emission bands of molecular oxygen *J. Chem. Phys.* **40** 1769–70
- Arnold J S, Browne R J and Ogryzlo E A 1965 The red emission bands of molecular oxygen *Photochem. Photobiol.* **4** 963–9
- Ashur I, Goldschmidt R, Pinkas I, Salomon Y, Szweczyk G, Sarna T and Scherz A 2009 Photocatalytic generation of oxygen radicals by the water-soluble bacteriochlorophyll derivative WST11, noncovalently bound to serum albumin *J. Phys. Chem.* **113** 8027–37
- Aubry J-M, Pierlot C, Rigaudy J and Schmidt R 2003 Reversible binding of oxygen to aromatic compounds *Acc. Chem. Res.* **36** 668–75
- Aveline B M, Hasan T and Redmond R W 1994 Photophysical and photosensitizing properties of benzoporphyrin derivative monoacid ring A (BPD-MA) *Photochem. Photobiol.* **59** 328–35

- Aveline B M, Sattler R M and Redmond R W 1998 Environmental effects on cellular photosensitization: correlation of phototoxicity mechanism with transient absorption spectroscopy measurements *Photochem. Photobiol.* **68** 51–62
- Azab M *et al* 2005 Verteporfin therapy of subfoveal minimally classic choroidal neovascularization in age-related macular degeneration: 2-year results of a randomized clinical trial *Arch. Ophthalmol.* **123** 448–57
- Baron E D, Malbasa C L, Santo-Domingo D, Fu P, Miller J D, Hannerman K K, Hsia A H, Oleinick N L, Colussi V C and Cooper K D 2010 Silicon phthalocyanine (pc 4) photodynamic therapy is a safe modality for cutaneous neoplasms: results of a phase 1 clinical trial *Lasers Surg. Med.* **42** 888–95
- Baumstark A L 1988 *Advances in Oxygenated Processes* ed A L Baumstark (Greenwich, CT: JAI Press) pp 31–84
- Bellnier D A, Greco W R, Loewen G M, Nava H, Oseroff A R, Pandey R K, Tsuchida T and Dougherty T J 2003 Population pharmacokinetics of the photodynamic therapy agent 2-[1-hexyloxyethyl]-2-devinyl pyropheophorbide-a in cancer patients *Cancer Res.* **63** 1806–13
- Bensasson R, Chachaty C, Land E J and Salet C 1972 Nanosecond irradiation studies of biological molecules—I. Coenzyme Q 6 (ubiquinone-30) *Photochem. Photobiol.* **16** 27–37
- Blay G, Garcia B, Molina E and Pedro J R 2005 Total syntheses of four stereoisomers of 4a-hydroxy-1b,7b-peroxy-10bH-guaia-5-ene *Org. Lett.* **7** 3291–4
- Bonnet R, Lambert C, Land E J, Scourides P A, Sinclair R S and Truscott T G 1983 The triplet and radical species of hematoporphyrin and some of its radical species *Photochem. Photobiol.* **38** 1–8
- Braslavsky S E and Heibel G E 1992 Time-resolved photothermal and photoacoustic methods applied to photoinduced processes in solution *Chem. Rev.* **92** 1381–410
- Cadet J, Douki T and Ravanat J L 2008 Oxidatively generated damage to the guanine moiety of DNA: mechanistic aspects and formation in cells *Acc. Chem. Res.* **41** 1075–83
- Cadet J, Ravanat J-L, Martinez G R, Medeiros M G H and Di Mascio P 2006 Singlet oxygen oxidation of isolated and cellular DNA: product formation and mechanistic insights *Photochem. Photobiol.* **82** 1219–25
- Catalan J, Diaz C and Barrio L 2003 Analysis of mixed solvent effects on the properties of singlet oxygen ($^1\Delta_g$) *Chem. Phys.* **300** 33–9
- Celaje J A, Zhang D, Guerrero A M and Selke M 2011 Chemistry of trans-resveratrol with singlet oxygen: [2 + 2] addition, [4 + 2] addition, and formation of the phytoalexin moracin M *Org. Lett.* **13** 4846–9
- Chakraborty A, Held K D, Prise K M, Liber H L and Redmond R W 2009 Bystander effects induced by diffusing mediators after photodynamic stress *Radiat. Res.* **172** 74–81
- Chattopadhyay S K, Kumar C V and Das P K 1984 Laser flash photolytic determination of triplet yields via singlet oxygen generation *J. Photochem.* **24** 1–9
- Chen B, Pogue B W, Zhou X, O'Hara J A, Solban N, Demidenko E, Hoopes P J and Hasan T 2005 Effect of tumor host microenvironment on photodynamic therapy in a rat prostate tumor model *Clin. Cancer Res.* **11** 720–7
- Chen Q, Wilson B C, Shetty S D, Patterson M S, Cerny J C and Hetzel F W 1997 Changes in *in vivo* optical properties and light distributions in normal canine prostate during photodynamic therapy *Radiat. Res.* **147** 86–91
- Clennan E L, Dobrowolski P and Greer A 1995 Reaction of singlet oxygen with thietane. a novel example of a self-catalyzed reaction which provides evidence for a thiadioxirane intermediate *J. Am. Chem. Soc.* **117** 9800–3
- Clennan E L and Foote C S 1992 *Organic Peroxides* ed W Ando (Chichester: Wiley) pp 255–318
- Cox G S, Bobillier C and Whitten D G 1982 Photooxidation and singlet oxygen sensitization by protoporphyrin IX and its photooxidation products *Photochem. Photobiol.* **36** 401–7
- Cox G S and Whitten D G 1982 Mechanisms for the photooxidation of protoporphyrin IX in solution *J. Am. Chem. Soc.* **104** 516–21
- Cuenca R E, Allison R R, Sibata C and Downie G H 2004 Breast cancer with chest wall progression: treatment with photodynamic therapy *Ann. Surg. Oncol.* **11** 322–7
- Demas J N and Crosby G A 1971 The measurement of photoluminescence quantum yields. Review *J. Phys. Chem.* **75** 991–1024
- Di Mascio P, Miyamoto S, Medeiros M G H, Martinez G R and Cadet J 2014 *Chemistry Functional Groups in Organic Chemistry—The Chemistry of Peroxides 3* ed S Patai and Z Rappoport (Chichester: John Wiley & Sons) pp 769–804
- Dougherty T J 1993 Photodynamic therapy *Photochem. Photobiol.* **58** 896–900

- Douki T, Riviere J and Cadet J 2002 DNA tandem lesions containing 8-oxo-7,8-dihydroguanine and formamido residues arise from intramolecular addition of thymine peroxy radical to guanine *Chem. Res. Toxicol.* **15** 445–54
- Dragieva G, Hafner J, Dummer R, Schmid-Grendelmeier P, Roos M, Prinz B M, Burg G, Binswanger U and Kempf W 2004 Topical photodynamic therapy in the treatment of actinic keratoses and Bowen's disease in transplant recipients *Transplantation* **77** 115–21
- Dysart J S and Patterson M S 2005 Characterization of photofrin photobleaching for singlet oxygen dose estimation during photodynamic therapy of MLL cells *in vitro* *Phys. Med. Biol.* **50** 2597–616
- Dysart J S and Patterson M S 2006 Photobleaching kinetics, photoproduct formation, and dose estimation during ALA induced PpIX PDT of MLL cells under well oxygenated and hypoxic conditions *Photochem. Photobiol. Sci.* **5** 73–81
- Dysart J S, Singh G and Patterson M S 2005 Calculation of singlet oxygen dose from photosensitizer fluorescence and photobleaching during mTHPC photodynamic therapy of MLL cells *Photochem. Photobiol.* **81** 196–205
- Ericson M B, Sandberg C, Stenquist B, Gudmunson F, Karisson M, Ros A-M, Rosen A, Larko O, Wennberg A-M and Rosdahl I 2004 Photodynamic therapy of actinic keratosis at varying fluence rates: assessment of photobleaching, pain and primary clinical outcome *Br. J. Dermatol.* **151** 1204–12
- Fernandez J M, Bilgin M D and Grossweiner L I 1997 Singlet oxygen generation by photodynamic agents *J. Photochem. Photobiol. B.* **37** 131–40
- Finlay J C, Conover D L, Hull E L and Foster T H 2001 Porphyrin bleaching and PDT-induced spectral changes are irradiance dependent in ALA-sensitized normal rat skin *in vivo* *Photochem. Photobiol.* **73** 54–63
- Finlay J C, Mitra S, Patterson M S and Foster T H 2004 Photobleaching kinetics of photofrin *in vivo* and in multicell tumour spheroids indicate two simultaneous bleaching mechanisms *Phys. Med. Biol.* **49** 4837–60
- Finlay J C, Zhu T C, Dimofte A, Stripp D, Malkowicz S B, Busch T M and Hahn S M 2006 Interstitial fluorescence spectroscopy in the human prostate during motexafin lutetium-mediated photodynamic therapy *Photochem. Photobiol.* **82** 1270–8
- Foote C S 1976 *Free Radicals in Biology* ed W A Pryor (New York: Academic) pp 85–133
- Foote C S 1991 Definition of type I and type II photosensitized oxidation *Photochem. Photobiol.* **54** 659
- Foster T H, Hartley D F, Nichols M G and Hilf R 1993 Fluence rate effects in photodynamic therapy of multicell tumor spheroids *Cancer Res.* **53** 1249–54
- Foster T H, Murant R S, Bryant R G, Knox R S, Gibson S L and Hilf R 1991 Oxygen consumption and diffusion effects in photodynamic therapy *Radiat. Res.* **126** 296–303
- Fudickar W and Linker T 2014 Applications of endoperoxides derived from acenes and singlet oxygen *The Chemistry of Peroxides* vol 3, ed A Greer and J F Liebman (Chichester: Wiley) pp 21–86
- Fuwa K and Valle B L 1963 The physical basis of analytical atomic absorption spectrometry. The pertinence of the Beer–Lambert law *Anal. Chem.* **35** 942–6
- Georgakoudi I and Foster T H 1998 Singlet oxygen- versus nonsinglet oxygen-mediated mechanisms of sensitizer photobleaching and their effects on photodynamic dosimetry *Photochem. Photobiol.* **67** 612–25
- Georgakoudi I, Nichols M G and Foster T H 1997 The mechanism of photofrin photobleaching and its consequences for photodynamic dosimetry *Photochem. Photobiol.* **65** 135–44
- Ghogare A A and Greer A 2016 Using singlet oxygen to synthesize natural products and drugs *Chem. Rev.* **116** 9994–10034
- Girotti A W 2001 Lipid photooxidative damage in biological membranes: reaction mechanisms, cytotoxic consequences, and defense strategies *Sun Protection in Man, Volume 3 (Comprehensive Series in Photosciences)* ed P U Giacomoni (Amsterdam: Elsevier) pp 231–50
- Gollmer A, Arnbjerg J, Blaikie F H, Wett Pedersen B, Breitenbach T, Daasbjerg K, Glasius M and Ogilby P R 2011 Singlet oxygen sensor green: photochemical behavior in solution and in a mammalian cell *Photochem. Photobiol.* **87** 671–9
- Gollnick K 1968 Type II photooxygenation reactions in solution *Advances in Photochemistry* vol 6, ed D H Volman, G S Hammond and K Gollnick (New York: Wiley) pp 1–122
- Greer A 2006 Christopher Foote's discovery of the role of singlet oxygen [$^1\text{O}_2$ ($^1\Delta_g$)] in photosensitized oxidation reactions *Acc. Chem. Res.* **39** 797–804
- Greer A, Balaban A T and Liebman J F 2014 *The Chemistry of Peroxides* vol 3 (Chichester: John Wiley & Sons, Ltd)

- Guldi D M, Mody T D, Gerasimchuk N N, Magda D and Sessler J L 2000 Influence of large metal cations on the photophysical properties of texaphyrin, a rigid aromatic chromophore *J. Am. Chem. Soc.* **122** 8289–98
- Hadjur C, Lange N, Rebstein J, Monnier P, van den Bergh H and Wagnieres G 1998 Spectroscopic studies of photobleaching and photoproduct formation of meta(tetrahydroxyphenyl)chlorin (m-THPC) used in photodynamic therapy. The production of singlet oxygen by m-THPC *J. Photochem. Photobiol. B* **45** 170–8
- Hage M, Siersema P D, van Dekken H, Steyerberg E W, Haringsma J, van de Vrie W, Grool T E, van Veen R L P, Sterenborg H J C M and Kulpers E J 2004 Aminolevulinic acid photodynamic therapy versus argon plasma coagulation for ablation of Barrett's oesophagus: a randomised trial *Gut* **53** 785–90
- He J, Larkin H E, Li Y-S, Rihter B D, Zaidi S I A, Rodgers M A J, Mukhtar H, Kenney M E and Oleinick N L 1997 The synthesis, photophysical and photobiological properties and *in vitro* structure-activity relationships of a set of silicon phthalocyanine PDT photosensitizers *Photochem. Photobiol.* **65** 581–6
- Hickerson R P, Prat F, Muller J G, Foote C S and Burrows C J 1999 Sequence and stacking dependence of 8-oxoguanine oxidation: comparison of one-electron versus singlet oxygen mechanisms *J. Am. Chem. Soc.* **121** 9423–8
- Higgins R, Foote C S and Cheng H 1968 *Advances in Chemistry* ed R F Gould (Washington DC: American Chemical Society) pp 102–17
- Hirano T, Kohno E and Nishiwaki M 2002 Detection of near infrared emission from singlet oxygen in PDT with an experimental tumor bearing mouse *J. Japan Soc. Laser Surg. Med.* **22** 99–108
- Hu X-H, Feng Y, Lu J Q, Allison R R, Cuenca R E, Downie G H and Sibata C H 2005 Modeling of a type II photofrin-mediated photodynamic therapy process in a heterogeneous tissue phantom *Photochem. Photobiol.* **81** 1460–8
- Huang Z 2005 A review of progress in clinical photodynamic therapy *Technol. Cancer Res. Treat.* **4** 283–93
- Hudson J A and Cater D B 1964 An analysis of factors affecting tissue oxygen tension *Proc. R. Soc. B* **161** 247–74
- Hurst J R, McDonald J D and Schuster G B 1982 Lifetime of singlet oxygen in solution directly determined by laser spectroscopy *J. Am. Chem. Soc.* **104** 2065–7
- Igbaseimokumo U 2004 Quantification of *in vivo* Photofrin uptake by human pituitary adenoma tissue *J. Neurosurg.* **101** 272–7
- Itri R, Junqueira H C, Mertins O and Babiata M S 2014 Membrane changes under oxidative stress: the impact of oxidized lipids *Biophys. Rev.* **6** 47–61
- Jarvi M T, Niedre M J, Patterson M S and Wilson B C 2006 Singlet oxygen luminescence dosimetry (SOLD) for photodynamic therapy: current status, challenges and future prospects *Photochem. Photobiol.* **82** 1198–210
- Jarvi M T, Niedre M J, Patterson M S and Wilson B C 2011 The influences of oxygen depletion and photosensitizer triplet-state dynamic during photodynamic therapy on accurate singlet oxygen luminescence monitoring and analysis of treatment dose response *Photochem. Photobiol.* **87** 223–34
- Jeffes E W B 2002 Levulan®: the first approved topical photosensitizer for the treatment of actinic keratosis *J. Dermatol. Treat.* **13** s19–23
- Jensen R L, Arnbjerg J and Ogilby P R 2010 Temperature effects on the solvent-dependent deactivation of singlet oxygen *J. Am. Chem. Soc.* **132** 8098–105
- Johansson A *et al* 2006 mTHPC pharmacokinetics following topical administration *Proc. SPIE* **6094** 60940C
- Josefsen L B and Boyle R W 2008 Photodynamic therapy and the development of metal-based photosensitisers *Met. Based Drugs* **2008** 1–24
- Kanofsky J R 1989 Singlet oxygen production by biological systems *Chem. Biol. Interact.* **70** 1–28
- Kanofsky J R 1990 Quenching of singlet oxygen by human plasma *Photochem. Photobiol.* **51** 299–303
- Kasha M 1985 *Singlet O₂* ed A A Frimer (Boca Raton, FL: CRC Press) pp 1–12
- Kato H *et al* 2003 Phase II clinical study of photodynamic therapy using mono-l-aspartyl chlorin *e*₆ and diode laser for early superficial squamous cell carcinoma of the lung *Lung Cancer* **42** 103–11
- Kelty C J, Ackroyd R, Brown N J, Brown S B and Reed M W 2004 Comparison of high- versus low-dose 5-aminolevulinic acid for photodynamic therapy of Barrett's esophagus *Surg. Endosc.* **18** 452–8
- Kennedy J C and Pottier R H 1992 Endogenous protoporphyrin IX, a clinically useful photosensitizer for photodynamic therapy *J. Photochem. Photobiol. B* **14** 275–92

- Khan A U and Kasha M 1963 Red chemiluminescence of molecular oxygen in aqueous solution *J. Chem. Phys.* **39** 2105–6
- Khan A U and Kasha M 1964 Rotational structure in the chemiluminescence spectrum of molecular oxygen in aqueous systems *Nature* **204** 241–3
- Khan A U and Kasha M 1970 Chemiluminescence arising from simultaneous transitions in pairs of singlet oxygen molecules *J. Am. Chem. Soc.* **92** 3293–300
- Khan A U and Kasha M 1979 Direct spectroscopic observation of singlet oxygen emission at 1268 nm excited by sensitizing dyes of biological interest in liquid solution *Proc. Natl Acad. Sci. USA* **76** 6047–9
- Kim M M, Penjweini R, Liang X and Zhu T C 2016 Explicit macroscopic singlet oxygen modeling for benzoporphyrin derivative monoacid ring A (BPD)-mediated photodynamic therapy *J. Photochem. Photobiol. B* **164** 314–22
- Kim M M, Liu B, Miller J, Busch T M and Zhu T C 2014a Parameter determination for BPD-mediated vascular PDT *Proc. SPIE* **8931** 89311D
- Kim M M, Penjweini R and Zhu T C 2015 *In vivo* outcome study of BPD-mediated PDT using a macroscopic singlet oxygen model *Proc. SPIE* **9308** 93080A
- Kim S, Ohulchanskyy T Y, Pudavar H E, Pandey R K and Prasad P N 2007 Organically modified silica nanoparticles co-encapsulating photosensitizing drug and aggregation-enhanced two-photon absorbing fluorescent dye aggregates for two-photon photodynamic therapy *J. Am. Chem. Soc.* **129** 2669–75
- Kim S, Tachikawa T, Fujitsuka M and Majima T 2014b Far-red fluorescence probe for monitoring singlet oxygen during photodynamic therapy *J. Am. Chem. Soc.* **136** 11707–15
- Kinsella T J *et al* 2011 Preliminary clinical and pharmacologic investigation of photodynamic therapy with the silicon phthalocyanine photosensitizer Pc 4 for primary or metastatic cutaneous cancers *Front. Oncol.* **1** 1–6
- Klaper M and Linker T 2015 Intramolecular transfer of singlet oxygen *J. Am. Chem. Soc.* **137** 13744–7
- Konig K, Schneckenburger H, Ruck A and Steiner R 1993 *In vivo* photoproduct formation during PDT with ALA-induced endogenous porphyrins *J. Photochem. Photobiol. B* **18** 287–90
- Kotani H, Ohkubo K and Fukuzumi S 2004 Photocatalytic oxygenation of anthracenes and olefins with dioxygen via selective radical coupling using 9-mesityl-10-methylacridinium ion as an effective electron-transfer photocatalyst *J. Am. Chem. Soc.* **126** 15999–6006
- Kotzabasaki V, Vassilikogiannakis G and Stratakis M 2016 Total synthesis and structural revision of (+)-yaoshanenolide *B. Org. Lett.* **18** 4982–5
- Krammer B and Plaetzer K 2008 ALA and its clinical impact, from bench to bedside *Photochem. Photobiol. Sci.* **7** 283–9
- Krasnovskii A A 1976 Photosensitized luminescence of singlet oxygen in solution *Biofizika* **21** 748–9
- Kress M, Meier T, Steiner R, Dolp F, Erdmann R, Ortmann U and Ruck A 2003 Time-resolved microspectrofluorometry and fluorescence lifetime imaging of photosensitizers using picosecond pulsed diode lasers in laser scanning microscopes *J. Biomed. Opt.* **8** 26–32
- Krieg M and Redmond R W 1993 Photophysical properties of 3,3'-dialkylthiacarbocyanine dyes in homogeneous solution *Photochem. Photobiol.* **57** 472–9
- Krieg M, Srichai M B and Redmond R W 1993 Photophysical properties of 3,3'-dialkylthiacarbocyanine dyes in organized media: unilamellar liposomes and thin polymer films *Biochim. Biophys. Acta* **1151** 168–74
- Lakowicz J R, Szmajcinski H, Nowaczyk K, Berndt K W and Johnson M 1992 Fluorescence lifetime imaging *Anal. Biochem.* **202** 316–30
- Lambert C and Redmond R W 1994 Triplet energy level of β -carotene *Chem. Phys. Lett.* **228** 495–8
- Lapini A *et al* 2012 A comparison of hexaminolevulinic acid (Hexvix) fluorescence cystoscopy and white-light cystoscopy for detection of bladder cancer: results of the HeRo observational study *Surg. Endosc.* **26** 3634–41
- Lee L K, Whitehurst C, Chen Q, Patelides M L, Hetzel F W and Moore J V 1997 Interstitial photodynamic therapy in the canine prostate *Br. J. Urol.* **80** 898–902
- Li L, Kodama K, Saito K and Aizawa K 2002 Phase-resolved fluorescence study of mono-L-aspartyl chlorin E_6 *J. Photochem. Photobiol. B* **67** 51–6
- Liang X, Wang K K and Zhu T C 2012 Singlet oxygen dosimetry modeling for photodynamic therapy *Proc. SPIE* **8210** 82100T
- Lin H, Shen Y, Chen D, Lin L, Wilson B C, Li B and Xie S 2013 Feasibility study on quantitative measurements of singlet oxygen generation using singlet oxygen sensor green *J. Fluoresc.* **23** 41–7

- Liu B, Farrell T J and Patterson M S 2012 Comparison of noninvasive photodynamic therapy dosimetry methods using a dynamic model of ALA-PDT of human skin *Phys. Med. Biol.* **57** 825–41
- Liu B, Kim M M, Gallagher-Colombo S M, Busch T M and Zhu T C 2014 Comparison of PDT parameters for RIF and H460 tumor models during HPPH-mediated PDT *Proc. SPIE* **8931** 89311C
- Liu B, Kim M M and Zhu T C 2013 A theoretical comparison of macroscopic and microscopic modeling of singlet oxygen during photofrin and HPPH-mediated PDT *Proc. SPIE* **8568** 856805
- Lovell J F, Liu T W, Chen J and Zheng G 2010 Activatable photosensitizers for imaging and therapy *Chem. Rev.* **110** 2839–57
- Lui H *et al* 2004 Photodynamic therapy of multiple nonmelanoma skin cancers with verteporfin and red light-emitting diodes *Arch. Dermatol.* **140** 26–32
- Lustig R A, Vogl T J, Fromm D, Cuenca R, Hsi R A, D’Cruz A K, Krajina Z, Turic M, Singhal A and Chen J C 2003 A multicenter phase I safety study of intratumoral photoactivation of talaporfin sodium in patients with refractory solid tumors *Cancer* **98** 1767–71
- Marks P V, Belchetz P E, Saxena A, Igbaseimokumo U, Thomson S, Nelson M, Stringer M R, Holroyd J A and Brown S B 2000 Effect of photodynamic therapy on recurrent pituitary adenomas: clinical phase III trial—an early report *Br. J. Neurosurg.* **14** 317–25
- Marti C, Nonell S, Nicolau M and Torres T 2000 Photophysical properties of neutral and cationic tetrapyrrolineporphyrins *Photochem. Photobiol.* **71** 53–9
- Mazor O, Brandis A, Plaks V, Neumark E, Rosenbach-Belkin V, Salomon Y and Scherz A 2005 WST11, a novel water-soluble bacteriochlorophyll derivative; cellular uptake, pharmacokinetics, biodistribution and vascular-targeted photodynamic activity using melanoma tumors as a model *Photochem. Photobiol.* **81** 342–51
- McCallum J E B, Kuniyoshi C Y and Foote C S 2004 Characterization of 5-hydroxy-8-oxo-7,8-dihydroguanosine in the photosensitized oxidation of 8-oxo-7,8-dihydroguanosine and its rearrangement to spiroiminodihydantoin *J. Am. Chem. Soc.* **126** 16777–82
- McDonagh A F 2001 Phototherapy: from ancient Egypt to the new millennium *J. Perinatol.* **21** S7–12
- McMillan D D, Chen D, Kim M M, Liang X and Zhu T C 2013 Parameter determination for singlet oxygen modeling of BPD-mediated PDT *Proc. SPIE* **8568** 856810
- Meng L, Wu Y and Yi T 2014 A ratiometric fluorescent probe for the detection of hydroxyl radicals in living cells *Chem. Commun.* **50** 4843–5
- Milanesio M E, Alvarez M G, Yslas E I, Borsarelli C D, Silber J J, Rivarola V and Durantini E N 2001 Photodynamic studies of metallo 5,10,15,20-tetrakis(4-methoxyphenyl) porphyrin: photochemical characterization and biological consequences in a human carcinoma cell line *Photochem. Photobiol.* **74** 14–21
- Miller J D, Baron E D, Scull H, Hsia A, Berlin J C, McCormick T, Colussi V, Kenney M E, Cooper K D and Oleinick N L 2007 Photodynamic therapy with the phthalocyanine photosensitizer Pc 4: the case experience with preclinical mechanistic and early clinical-translational studies *Toxicol. Appl. Pharm.* **224** 290–9
- Mitra S and Foster T H 2005 Photophysical parameters, photosensitizer retention and tissue optical properties completely account for the higher photodynamic efficacy of meso-tetra-hydroxyphenylchlorin versus photofrin *Photochem. Photobiol.* **81** 849–59
- Moan J and Berg K 1991 The photodegradation of porphyrins in cells can be used to estimate the lifetime of singlet oxygen *Photochem. Photobiol.* **53** 549–53
- Mody T D 2000 Pharmaceutical development and medical applications of porphyrin-type macrocycles *J. Porphyr. Phthalocya.* **4** 362–7
- Momma T, Hamblin M R, Wu H C and Hasan T 1998 Photodynamic therapy of orthotopic prostate cancer with benzoporphyrin derivative: local control and distant metastasis *Cancer Res.* **58** 5425–31
- Musbat L, Weitman H and Ehrenberg B 2013 Azide quenching of singlet oxygen in suspensions of microenvironments of neutral and surface charged liposomes and micelles *Photochem. Photobiol.* **89** 253–8
- Nichols M G and Foster T H 1994 Oxygen diffusion and reaction kinetics in the photodynamic therapy of multicell tumour spheroids *Phys. Med. Biol.* **39** 2161–81
- Niedre M J, Patterson M S and Wilson B C 2002 Direct near-infrared luminescence detection of singlet oxygen generated by photodynamic therapy in cells *in vitro* and tissues *in vivo* *Photochem. Photobiol.* **75** 382–91
- Nyokong T 2007 Effects of substituents on the photochemical and photophysical properties of main group metal phthalocyanines *Coord. Chem. Rev.* **251** 1707–22

- Ogilby P R and Foote C S 1983 Chemistry of singlet oxygen. 42. Effect of solvent, solvent isotopic substitution, and temperature on the lifetime of singlet molecular oxygen ($^1\Delta_g$) *J. Am. Chem. Soc.* **105** 3423–30
- Ohkubo K, Nanjo T and Fukuzumi S 2005 Efficient photocatalytic oxygenation of aromatic alkene to 1,2-dioxetane with oxygen via electron transfer *Org. Lett.* **7** 4265–8
- Ohmori S and Arai T 2006 *In vitro* behavior of Porfimer sodium and Talaporfin sodium with high intensity pulsed irradiation *Lasers Med. Sci.* **21** 213–23
- Ohmori S, Hakomori S and Arai T 2007 Flow rate and fluence rate dependences of the triplet-state lifetime of talaporfin sodium photochemical reaction in flowing solution *Japan. J. Appl. Phys.* **46** 1217–9
- Ormond A B and Freeman H S 2013 Dye sensitizers for photodynamic therapy *Materials* **6** 817–40
- Ouedraogo G D and Redmond R W 2003 Secondary reactive oxygen species extend the range of photosensitization effects in cells: DNA damage produced via initial membrane photosensitization *Photochem. Photobiol.* **77** 192–203
- Pandey R K, Sumlin A B, Constantine S, Aoudia M, Potter W R, Bellnier D A, Henderson B W, Rodgers M A J, Smith K M and Dougherty T J 1996 Alkyl ether analogs of chlorophyll-a derivatives: part I. synthesis, photophysical properties and photodynamic efficacy *Photochem. Photobiol.* **64** 194–204
- Patterson M S, Madsen S J and Wilson B C 1990 Experimental tests of the feasibility of singlet oxygen luminescence monitoring *in vivo* during photodynamic therapy *J. Photochem. Photobiol. B* **5** 69–84
- Pedersen S K, Jolmehave J, Blaikie F H, Gollmer A, Breitenbach T, Jensen H H and Ogilby P R 2014 Aarhus sensor green: a fluorescent probe for singlet oxygen *J. Org. Chem.* **79** 3079–87
- Penjweini R, Kim M M and Zhu T C 2015a *In vivo* outcome study of HPPH mediated PDT using singlet oxygen explicit dosimetry (SOED) *Proc. SPIE* **9308** 93080N
- Penjweini R, Liu B, Kim M M and Zhu T C 2015b Explicit dosimetry for 2-(1-Hexyloxyethyl)-2-devinyl pyropheophorbide-a (HPPH) mediated photodynamic therapy: macroscopic singlet oxygen modeling *J. Biomed. Opt.* **20** 128003
- Plaetzer K, Krammer B, Berlanda J, Berr F and Kiesslich T 2009 Photophysics and photochemistry of photodynamic therapy: fundamental aspects *Lasers Med. Sci.* **24** 259–68
- Pogue B W, Elliott J T, Kanick S C, Davis S C, Samkoe K S, Maytin E V, Pereira S P and Hasan T 2016 Revisiting photodynamic therapy dosimetry: reductionist and surrogate approaches to facilitate clinical success *Phys. Med. Biol.* **61** R57–89
- Poole D C, Behnke B J, McDonough P, McAllister R M and Wilson D F 2004 Measurement of muscle microvascular oxygen pressures: compartmentalization of phosphorescent probe *Microcirculation* **11** 317–26
- Pouget J-P, Douki T, Richard M-J and Cadet J 2000 DNA damage induced by cells by γ and UVA radiation as measured by HPLC/GC-MS and HPLC-EC and comet assay *Chem. Res. Toxicol.* **13** 541–9
- Price M, Heilbrun L and Kessel D 2013 Effects of the oxygenation level on formation of different reactive oxygen species during photodynamic therapy *Photochem. Photobiol.* **89** 683–6
- Price M, Reiners J J, Santiago A M and Kessel D 2009 Monitoring singlet oxygen and hydroxyl radical formation with fluorescent probes during photodynamic therapy *Photochem. Photobiol.* **85** 1177–81
- Qiu H, Kim M M, Penjweini R and Zhu T C 2016 Macroscopic singlet oxygen modeling for dosimetry of Photofrin-mediated photodynamic therapy—an *in-vivo* study *J. Biomed. Opt.* **21** 088002
- Ragas X, Jimenez-Banzo A, Sanchez-Garcia D, Batllori X and Nonell S 2009 Singlet oxygen photosensitisation by the fluorescent probe singlet oxygen sensor green[®] *Chem. Commun.* **20** 2920–2
- Ranby B 1981 The history of singlet oxygen—an introduction *Kem. Tidskr.* **93** 36–7
- Redmond R W and Gamlin J N 1999 A compilation of singlet oxygen yields from biologically relevant molecules *Photochem. Photobiol.* **70** 391–475
- Robinson D J, de Bruijn H S, van der Veen N, Stringer M R, Brown S B and Star W M 1998 Fluorescence photobleaching of ALA-induced protoporphyrin IX during photodynamic therapy of normal hairless mouse skin: the effect of light dose and irradiance and the resulting biological effect *Photochem. Photobiol.* **67** 140–9
- Rodgers M A J and Lee P C 1984 Singlet molecular oxygen in micellar systems. 2. Quenching behavior in AOT reverse micelles *J. Phys. Chem.* **88** 3480–4
- Russell J A, Diamond K R, Collins T J, Tiedje H F, Hayward J E, Farrell T J, Patterson M S and Fang Q 2008 Characterization of fluorescence lifetime of photofrin and delta-aminolevulinic acid

- induced protoporphyrin IX in living cells using single- and two-photon excitation *IEEE J. Sel. Top. Quantum. Electron.* **14** 158–66
- Setsukinai K, Urano Y, Kakinuma K, Majima H J and Nagano T 2003 Development of novel fluorescence probes that can reliably detect reactive oxygen species and distinguish specific species *J. Biol. Chem.* **278** 3170–5
- Sharman W M, Allen C M and van Lier J E 2000 Role of activated oxygen species in photodynamic therapy *Methods Enzymol.* **319** 376–400
- Sheu C and Foote C S 1993 Endoperoxide formation in a guanosine derivative *J. Am. Chem. Soc.* **115** 10446–7
- Shonat R D and Kight A C 2003 Oxygen tension imaging in the mouse retina *Ann. Biomed. Eng.* **31** 1084–96
- Simone C B, Friedberg J S, Glatstein E, Stevenson J P, Sterman D H, Hahn S M and Cengel K A 2012 Photodynamic therapy for the treatment of non-small cell lung cancer *J. Thorac. Dis.* **4** 63–75
- Spikes J D and Bommer J C 1993a Photobleaching of mono-L-aspartyl chlorine e_6 (NP e_6): a candidate sensitizer for the photodynamic therapy of tumors *Photochem. Photobiol.* **58** 346–50
- Spikes J D and Bommer J C 1993b Photosensitizing properties of mono-L-aspartyl chlorine e_6 (NP e_6): a candidate sensitizer for the photodynamic therapy of tumors *J. Photochem. Photobiol. B* **17** 135–43
- Sporn L A and Foster T H 1992 Photofrin and light induces microtubule depolymerization in cultured human endothelial cells *Cancer Res.* **52** 3443–8
- Sterenborg H J C M and van Gemert M J C 1996 Photodynamic therapy with pulsed light sources: a theoretical analysis *Phys. Med. Biol.* **41** 835–49
- Stratakis M and Orfanopoulos M 2000 Regioselectivity in the ene reaction of singlet oxygen with alkenes *Tetrahedron* **56** 1595–615
- Strickler S J and Berg R A 1962 Relationship between absorption intensity and fluorescence lifetime of molecules *J. Chem. Phys.* **37** 814–22
- Stripp D C H *et al* 2004 Phase I trial of motexafin-lutetium-mediated interstitial photodynamic therapy in patients with locally recurrent prostate cancer *Proc. SPIE* **5315** 88–99
- Touma D, Yarr M, Whitehead S, Konnikov N and Gilchrest B A 2004 A trial of short incubation, broad-area photodynamic therapy for facial actinic keratoses and diffuse photodamage *Arch. Dermatol.* **40** 33–40
- Turro N J, Ramamurthy V and Scaiano J C 2010 *Modern Molecular Photochemistry of Organic Molecules* (Sausalito, CA: University Science Book) pp 1001–40
- Vakrat-Haglili Y *et al* 2005 The microenvironment effect on the generation of reactive oxygen species by Pd-bacteriopheophorbide *J. Am. Chem. Soc.* **127** 6487–97
- Vassilikogiannakis G, Margaros I, Montagnon T and Stratakis M 2005 Illustrating the power of singlet oxygen chemistry in a synthetic context: biomimetic syntheses of litseaverticillols A–G, I and J and the structural reassignment of litseaverticillol E *Chem. Eur. J.* **11** 5899–907
- Verigos K *et al* 2006 Updated results of a phase I trial of motexafin lutetium-mediated interstitial photodynamic therapy in patients with locally recurrent prostate cancer *J. Environ. Pathol. Toxicol. Oncol.* **25** 373–88
- Walsh A 1955 The application of atomic absorption spectra to chemical analysis *Spectrochimica Acta* **7** 108–17
- Wang K K, Finlay J C, Busch T M, Hahn S M and Zhu T C 2010 Explicit dosimetry for photodynamic therapy: macroscopic singlet oxygen modeling *J. Biophoton.* **3** 304–18
- Wang K K, Mitra S and Foster T H 2007 A comprehensive mathematical model of microscopic dose deposition in photodynamic therapy *Med. Phys.* **34** 282–93
- Wasserman H H and Murray R W (ed) 1979 *Singlet Oxygen* vol 40 (New York: Academic)
- Wasserman H H and Larsen D L 1972 Formation of 1,4-endoperoxides from the dye-sensitized photo-oxygenation of alkylnaphthalenes *J. Chem. Soc. Chem. Commun.* 253–4
- Weersink R A, Bogaards A, Gertner M, Davidson S R H, Zhang K, Netchev G, Trachtenberg J and Wilson B C 2005a Techniques for delivery and monitoring of TOOKAD (WST09)-mediated photodynamic therapy of the prostate: clinical experience and practicalities *J. Photochem. Photobiol. B* **79** 211–22
- Weersink R A, Forbes J, Bisland S, Trachtenberg J, Elhilali M, Brun P H and Wilson B C 2005b Assessment of cutaneous photosensitivity of TOOKAD (WST09) in preclinical animal models and in patients *Photochem. Photobiol.* **81** 106–13
- Weishaupt K R, Gomer C J and Dougherty T J 1976 Identification of singlet oxygen as the cytotoxic agent in photo-activation of a murine tumor *Can. Res.* **36** 2326–92

- Weldon D, Poulsen T D, Mikkelsen K V and Ogilby P R 1999 Singlet sigma: the 'other' singlet oxygen in solution *Photochem. Photobiol.* **70** 369–79
- Wessels J M and Rodgers M A J 1995 Detection of the $O_2(^1\Delta_g)-O_2(^3\Sigma_g^-)$ transition in aqueous environments: a Fourier-transform near-infrared luminescence study *J. Phys. Chem.* **99** 15725–7
- Weston M A and Patterson M S 2011 Calculation of singlet oxygen dose using explicit and implicit dose metrics during benzoporphyrin derivative monoacid ring A (BPD-MA)-PDT *in vitro* and correlation with MLL cell survival *Photochem. Photobiol.* **87** 1129–37
- Wezgowiec J, Derylo M B, Teissie J, Orio J, Rols M-P, Kulbacka J, Saczko J and Kotulska M 2013 Electric field-assisted delivery of photofrin to human breast carcinoma cells *J. Membrane Biol.* **246** 725–35
- Wiedmann M, Berr F, Schiefke I, Witzigmann H, Kohlhaw K, Mossner J and Caca K 2004 Photodynamic therapy in patients with non-resectable hilar cholangiocarcinoma: 5 year follow-up of a prospective phase II study *Gastrointest. Endosc.* **60** 68–75
- Wiedmann M, Caca K, Berr F, Schiefke I, Tannapfel A, Wittekind C, Mossner J, Hauss J and Witzigmann H 2003 Neoadjuvant photodynamic therapy as a new approach to treating hilar cholangiocarcinoma: a phase II pilot study *Cancer* **97** 2783–90
- Wilkinson F and Brummer J G 1981 Rate constants for the decay and reactions of the lowest electronically excited singlet state of molecular oxygen in solution *J. Phys. Chem. Ref. Data* **10** 809–999
- Wilkinson F, Helman W P and Ross A B 1993 Quantum yields for the photosensitized formation of the lowest electronically excited singlet state of molecular oxygen in solution *J. Phys. Chem. Ref. Data* **22** 113–262
- Wilson B C and Patterson M S 2008 The physics, biophysics, and technology of photodynamic therapy *Phys. Med. Biol.* **53** R61–109
- Yapici N B, Jockusch S, Moscatelli A, Mandalapu S R, Itagaki Y, Bates D K, Weiseman S, Gibson K M, Turro N J and Bi L 2012 New rhodamine nitroxide based fluorescent probes for intracellular hydroxyl radical identification in living cells *Org. Lett.* **14** 50–3
- Yuan L, Lin W and Song J 2010 Ratiometric fluorescent detection of intracellular hydroxyl radicals based on a hybrid coumarin–cyanine platform *Chem. Commun.* **46** 7930–2
- Zaklika K A, Thayer A L and Schaap A P 1978 Substituent effects on the decomposition of 1,2-dioxetanes *J. Am. Chem. Soc.* **100** 4916–8
- Zamadar M and Greer A 2010 *Handbook of Synthetic Photochemistry* ed A Albini and M Fagnoni (Weinheim: Wiley) pp 353–86
- Zhao B, Yin J, Bilski P J, Chignell C F, Roberts J E and He Y 2009 Enhanced photodynamic efficacy towards melanoma cells by encapsulation of Pc4 in silica nanoparticles *Toxicol. Appl. Pharm.* **241** 163–72
- Zhu T C and Finlay J C 2008 The role of photodynamic therapy (PDT) physics *Med. Phys.* **35** 3127–36
- Zhu T C, Finlay J C and Hahn S M 2005 Determination of the distribution of light, optical properties, drug concentration, and tissue oxygenation *in vivo* in human prostate during motexafin lutetium-mediated photodynamic therapy *Photochem. Photobiol.* **79** 231–41
- Zhu T C, Finlay J C, Zhou X and Li J 2007 Macroscopic modeling of the singlet oxygen production during PDT *Proc. SPIE* **6427** 642708
- Zhu T C, Hahn S M, Kapatkin A S, Dimofte A, Rodriguez C E, Vulcan T G, Glatstein E and Hsi R A 2003 *In vivo* optical properties of normal canine prostate at 732nm using motexafin lutetium-mediated photodynamic therapy *Photochem. Photobiol.* **77** 81–8
- Zhu T C, Kim M M, Liang X, Finlay J C and Busch T M 2015a *In vivo* singlet oxygen threshold doses for PDT *Photon Lasers Med.* **4** 59–71
- Zhu T C, Liu B and Kim M M 2015b Computer models of the dynamic processes in photodynamic therapy *Computational Bioengineering* ed G Zhang (Boca Raton, FL: CRC Press) pp 231–64
- Zhu T C and Liu B 2013 Singlet oxygen modeling of PDT incorporating local vascular oxygen diffusion *Proc. COMSOL User Conf.* pp 1–4
- Zhu T C, Liu B, Kim M M, McMillan D D, Liang X, Finlay J C and Busch T M 2014 Comparison of singlet oxygen threshold doses for PDT *Proc. SPIE* **8931** 89310I
- Zhu T C, Liu B and Penjweini R 2015c Study of tissue oxygen supply rate in a macroscopic photodynamic therapy singlet oxygen model *J. Biomed. Opt.* **20** 038001